

1 **Imaging of the electrical activity in the root zone under limited water**
2 **availability stress: A laboratory study for *Vitis vinifera*.**

3 Benjamin Mary^{1,2}, Veronika Iván¹, Franco Meggio^{3,4}, Luca Peruzzo^{1,2}, Guillaume Blanchy⁵, Chunwei
4 Chou², Benedetto Ruperti^{3,4}, Yuxin Wu², Giorgio Cassiani¹

5 ¹Dipartimento di Geoscienze, Università degli Studi di Padova, Padova, Italy

6 ²Earth and Environmental Sciences Area, Lawrence Berkeley National Laboratory, California, USA

7 ³Department of Agronomy, Food, Natural resources, Animals and Environment – DAFNAE, University of Padova, Agripolis,
8 Viale dell'Università 16 – Legnaro (Padova), Italy;

9 ⁴Interdepartmental Research Centre for Viticulture and Enology - CIRVE, University of Padova, Via XXVIII Aprile 14,
10 Conegliano (Treviso), Italy;

11 ⁵Urban and Environmental Engineering, University of Liège (ULiege), Liège, Belgium

12

13 *Correspondence to:* B. Mary (benjamin.mary@unipd.it)

14 **Abstract**

15 Understanding root signals and their consequences on the whole plant physiology is one of the keys to tackling the water-
16 saving challenge in agriculture. The implementation of water-saving irrigation strategies, such as the partial root-zone drying
17 (PRD) method, as part of a comprehensive approach to enhance water use efficiency. To reach this goal tools are needed for
18 the evaluation of the root's and soil water dynamics in time and space. In controlled laboratory conditions, using a rhizotron
19 built for geoelectrical tomography imaging, we monitored the spatio-temporal changes in soil electrical resistivity (ER) for
20 more than a month corresponding to 8 alternating water inputs cycles. Electrical Resistivity Tomography (ERT) was
21 complemented with Electrical Current Imaging (ECI) using plant stem-induced electrical stimulation. To estimate soil water
22 content in the rhizotron during the experiment, we incorporated Archie's law as a constitutive model. We demonstrated that
23 under mild water stress conditions, it is practically impossible to spatially distinguish the limited water availability effects
24 using ECI. We evidenced that the Current Source Density spatial distribution varied during the course of the experiment with

25 the transpiration demand but without any significant relationship to the soil water content changes . On the other hand, ERT
26 showed spatial patterns associated with irrigation and, to a lesser degree, to RWU and hydraulic redistribution. The
27 interpretation of the geoelectrical imaging with respect to root activity was strengthened and correlated with indirect
28 observations of the plant transpiration using a weight monitoring lysimeter and direct observation of the plant leaf gas
29 exchanges.

30 **1. Introduction**

31 In the context of water scarcity, agriculture needs to improve irrigation practices by reducing water inputs and selecting
32 adequate species and, in the case of woody crops, most efficient scion-rootstock combinations. In order to evaluate the efficacy
33 of irrigation, it is necessary to develop tools capable of evaluating root functioning and quantifying root water uptake. The
34 partial root zone drying (PRD) and RDI (Regulated Deficit Irrigation) methods are part of an ensemble of deficit irrigation (DI)
35 strategies that aim at improving water use efficiency. The PRD, for instance, consists of irrigating only one part of the root
36 system of the same plant using a certain percentage of the potential evapotranspiration (ET_p), usually inferior to the total water
37 needed. Application of DI triggers a physiological response in the plant via a hormone called Abscisic acid (ABA), which is
38 produced in the roots and transmitted to the leaves to regulate the stomata closure and thus reducing water transpiration while
39 keeping photosynthesis active and finally leading to increased water use efficiency (as reviewed in Loveys et al., 2000; Davies
40 et al., 2002). Notably, if there is adequate sap flow through the roots, the ABA signal is transmitted through the xylem to the
41 leaf, as demonstrated by Dodd et al. (2008). According to Davies and Hartung (2004), it is proposed that plants subjected to
42 partial root-zone drying (PRD) demonstrate improved performance compared to plants under deficit irrigation (DI) when an
43 equal amount of water is applied. This is attributed to the ability of PRD to stimulate root growth and maintain consistent
44 signalling of abscisic acid (ABA) to regulate shoot physiology. Davies and Hartung (2004) stated that the effects of PRD on
45 plant growth, yielding and functioning are quantitatively different from those of RDI. One of the advantages of PRD when
46 operated properly, is that plants sustained and even increased shoot and fruit turgor even though a reduced amount of water is
47 applied to roots (Mingo et al., 2003). On the other hand, one of the disadvantages of RDI is that the entire root zone is allowed
48 to dry out, the roots can become stressed and damaged and if not rewetted can die and signalling may diminish. Conversely

49 Fernández et al. (2006) stated that not always a PRD treatment has been found advantageous as compared to a companion
50 regulated deficit irrigation (RDI) treatment and demonstrated it in a study on olive trees in which sap flow measurements,
51 which reflected water use throughout the irrigation period, showed no evidence of stomatal conductance being more reduced
52 in PRD than in RDI trees. Collins et al. (2009), in an experiment on the grapevine (*Vitis vinifera* L.) show that the response to
53 PRD applied at 100% ETC and deficit irrigation applied at 65% ETC was the same, increasing stomatal sensitivity to vapour
54 pressure deficit and decreasing sap flow. According to Cai et al. (2022), while stomatal conductance is a significant
55 aboveground hydraulic factor influencing water use in crops, it should not discount the role of belowground hydraulics, as
56 changes in soil-plant hydraulic conductance have been found to drive stomatal closure (Abdalla et al., 2021). This highlights
57 the crucial importance of studying electrical activity in the soil.

58 The plant's natural bioelectrical activity is necessary for its physiological processes. Plant scientists represent it by a water
59 column where the ions move from bottom to top and vice versa due to gradients of water potentials. In their studies, Voytek
60 et al. (2019) and Gibert et al. (2006) successfully linked the measurements of electrical potential in the ground and in the tree
61 stem to the RWU and sap flow respectively. The use of active methods such as electrical resistivity tomography (ERT) allows
62 for spatial and temporal analysis of the subsoil. Recent advances in electrical tomography imaging, in particular reduced at the
63 plant scale, show their effectiveness to measure changes in soil water content associated with the RWU (e.g. Cassiani et al.,
64 2015, 2016; Mary et al., 2018). Note that the correlation between root water uptake and soil water content changes exists when
65 averaged over a larger spatial scale than the scale at which soil moisture redistribution can compensate for local root activity.
66 The determination of these spatial scales depends on the soil hydraulic properties. This correlation between root water uptake
67 and changes in soil water content can also be influenced by the time scales in addition to spatial scales. The ability to
68 discriminate between them relies on factors such as the soil hydraulic properties, rates of local water extraction, and the
69 temporal dynamics of water redistribution in the soil (Anonymous Reviewer, 2023). Applications of geoelectrical methods to
70 evaluate water use efficiency are increasing. Recently in an experimental Citrus orchard, Consoli et al., (2017), Vanella et al.,
71 2018 and Mary et al., (2019a) showed that the observed drying pattern resulting from an elevated evapotranspiration rate (ER)
72 in the non-irrigated section of the root zone matches the root distribution in that area, while the observed wetting pattern arising
73 from a decreased ER in the irrigated section of the root zone can be attributed to the irrigation itself.

74 However, processes occurring in the rhizosphere can affect the soil ER in various ways. Roots induce changes in the soil
75 structure in terms of porosity and hydraulic conductivity which ultimately modify the water pathways and fluxes and thus the
76 ER itself. Soil structure changes may have a relatively smaller effect on ER than root water uptake RWU, although this may
77 differ for species with extensive root systems like woody species; this is further true during rainfall or irrigation considering
78 water redistribution and channelling influenced by varying root anatomies and causing dynamic variations in ER. Stemflow
79 channelling by roots is an example of how water from rain or irrigation can be driven to soil recharge by the root structure.
80 Conversely, root uplift in agroforestry shows how water can move from the deeper layers to the top via the roots. Roots also
81 affect the soil ER through the geochemical changes associated with root exudates and root symbiosis. At the interface between
82 soil and roots, the chemical gradients and concentrations can drastically differ from those observed in the soil regions not
83 affected by the roots. Although this can have a significant impact and be a valuable source of information, only a few studies
84 have extended the ERT and the induced polarisation (IP) to observe these changes (Weigand, 2017; Weigand and Kemna,
85 2019; Tsukanov and Schwartz, 2020, 2021). As of today, the electrical behaviour of individual roots remains poorly
86 understood, particularly with regard to their changes in type (from hair roots to fully lignified roots), space, time, and whether
87 the root is active or not (Ehosioko et al., 2020).

88 The geophysical approach extends the scope of traditional methods to evaluate soil water content (SWC) using time-domain
89 reflectometry (TDR) sensors and the calculation of RWU (Jackisch et al., 2020). In the field, the spatial resolution is controlled
90 (in ERT or IP) by the arrangement of the electrodes and acquisition parameters (Uhlemann et al., 2018), while the temporal
91 resolution is controlled by the time it takes to complete a full sequence measurement.

92 Rhizotrons are one of the earliest and most effective tools for studying root growth and functioning, both in the field and in
93 the laboratory (Taylor et al., 1990). They are transparent boxes that allow the direct observation of the roots during plant
94 growth and changes in soil conditions. Rhizotrons also provide valuable support in multidisciplinary studies, allowing other
95 methods to be more easily and precisely deployed, so that their results more reliably interpreted. For example, a load scale is
96 often mounted in combination with the rhizotron in order to weigh the system, which allows inferring the quantity of water
97 lost by the plant over time. This set-up is inspired by the lysimeter and is widely adopted to measure the water balance of the

98 soil-plant interactions. For example, in a rhizotron, Doussan and Garrigues (2019) use the light transmission 2D technique to
99 infer root water uptake with respect to their genotypes.

100 The very few studies conducting geophysical tomography imaging in the laboratory using a rhizotron proved a certain
101 efficiency in studying the interaction between soil physics and plant physiology for predicting plant response to environmental
102 stresses (Weigand, 2017, 2019; Peruzzo et al., 2020). It allows for high-resolution tomography by reducing the size, diameter,
103 and spacing of the electrodes. The entire soil profile is easily accessible by placing electrodes on the side of the rhizotron,
104 easing the depth resolution limitation inherent to surface-based geophysical methods usually used for field acquisition.

105 Although there is a good momentum for the use of geophysical methods applied to agronomy (Garré et al., 2021), a number
106 of gaps still need to be addressed. All the indirect root effects on the soil ER affect the evaluation of the soil water content,
107 making the interpretation of ERT to quantify RWU sometimes difficult (Ehosioko et al., 2020).

108 **1.1. Current pathways in roots under water stress constraints**

109 Current pathways in roots remain certainly the main unknown since there is a gap in techniques to measure
110 it non-destructively (Ehosioko et al., 2020; Liu et al., 2021). The current pathways in roots are possibly
111 linked to RWU. Lovisolo et al. (2016) describe in detail the flow of water from root water uptake and the
112 processes occurring at the cell scale. In any case, root water uptake is not distributed equally over the whole
113 root system, in part, due to heterogeneous soil conditions. For the same reason as soil saturation can change
114 over time, RWU is also varying in the time. The concept of active roots has been previously employed by
115 several authors (Frensch and Steudle, 1989; Doussan et al., 1998; Garrigues et al., 2006; Srayeddin and
116 Doussan, 2009) to characterise the spatial variability of root water uptake. In this context, plants adapt by
117 reducing radial conductivity in dry regions, enabling them to redirect their uptake towards wetter areas with
118 higher soil conductivity. This mechanism allows plants to maintain a consistent rate of water uptake while
119 sustaining higher plant water potentials. For active roots, root water uptake consists in a moving water from
120 the root tip (which is usually much more electrically conductive due to high water conductivity at its
121 proximity) in the radial direction via cellular (symplastic way) and between cells (apoplastic way) until it
122 reaches the xylem which transport it in the axial direction towards the upper part. Water flow can encounter

123 resistances due to suberization (conversion of the cell walls into cork tissue by development of suberin),
124 which is naturally driven as a consequence of root growth (secondary roots are more suberised than primary
125 roots) but it can also be the consequence of plant stress (Malavasi et al., 2016; Song et al., 2019). The process
126 can cause reductions in water conductivity through the root system by limiting the permeability of the root
127 tissue, thus leading to changes in the plant's ability to take up water. Aroca et al. (2012) describes in a generic
128 manner the plant responses to drought stress. For the specific PRD case, there is a complex tradeoff induced
129 by root suberization between reducing radial flow (as a consequence of ABA signalling sent by the roots) to
130 conserve water in the soil but keeping the axial flow active. This can be done for instance by adjusting the
131 xylem vessels size and quantities. Although suberisation is usually a long-term process, studies show that
132 PRD can promote and accelerate the process of suberization in response to water limitation. Finally during
133 PRD conditions we can also observe transfer of water from the wet to the dry side through the roots
134 (overnight) in a process called redistribution (Yan et al., 2020), which induces spatio-temporal variations in
135 RWU that ultimately also influences electrical current pathways in roots.

136 A direct approach to analysing the active part of the root system consists of an injection of current stimuli
137 into the plant stem. There is a variety of stem based methods used in the literature with applications ranging
138 from biomass estimation, root morphology to root physiology (root activity). At a single frequency, we
139 distinguish between ECM methods which rely on capacitance measurements and are commonly used to
140 study root systems at the plant scale and EIM, which measures both capacitance and resistance. Capacitance
141 represents the polarization processes and measures the charges stored during the current flow. Both use the
142 fact that the root can polarise at the soil-root interface and inside the root to infer direct root-related
143 information such as dry and wet mass, surface area,...). A second group of methods Electrode Impedance
144 Spectroscopy (EIS) uses a range of frequencies to capture the polarisation processes sensitive to the root
145 physiology and anatomy. For a detailed description of the methods, the reader is invited to refer to (Ehosioko
146 et al., 2020). The stem based approach has been developed for years by plant physiologists, starting from the
147 theory developed by Dalton (1995) who conceptualized the current pathways through the root xylem by an

148 equivalent parallel resistance-capacitance circuit. The theory holds under the assumption that the current
149 flows throughout the most conductive path and is held (thus inducing polarization) by the root cell
150 membranes before being released into the soil. Fine root connections and mycorrhiza facilitate the efficient
151 transfer of injected current into the soil at contact points between roots and the soil, resulting in a distribution
152 of current sources within the ground. Contrasting experimental results have challenged the relationship
153 between root electrical capacitance and root traits in different crops, with studies highlighting the potential
154 contribution of the stem, rather than the roots, to the overall measured root electrical capacitance and the
155 occurrence of current leakage at the proximal part (Urban et al., 2011; Dietrich et al., 2018; Peruzzo et al.,
156 2020).

157 Without being able yet to give hints about the electrical current pathway, recent advancements in the
158 development of explicit RWU models, based on plant hydraulics, provide insights into how robust
159 capacitance models hold and under which conditions. We learnt, for instance, that at the root level, RWU
160 models account for the anisotropy by separating the root hydraulic conductance into two terms i.e. axial and
161 radial (Javaux et al., 2008; Couvreur et al., 2012). According to Fig.1 In dry soil, the gradient $\Delta\psi_{\text{soil}} = (\psi_{\text{soil}} -$
162 $\psi_{\text{soil-root}})$ is higher than in wet soil. As the soil conductance g_s is linked by the relationship between the
163 transpiration rate over the $\Delta\psi_{\text{soil}}$, for the same evaporation rate, g_s is increasing when the soil dries out.
164 For a constant soil conductance, when the evaporation rate is increasing the g_s increase. The same occurs
165 for the root conductance g_r . The root axial water flow rates Q_x (L3T⁻¹) and root radial water flow rates Q_r
166 (L3T⁻¹) can be solved analytically by solving the system of equations of Ohm's and Kirchhoff's laws
167 (Couvreur et al., 2012)

168
169 The same applies to the stem-based methods as root hydraulic conductance and electrical conductivity are
170 likely to vary conjointly. Up to now the relationship between root water content and root hydraulic
171 conductivity with ER has not been firmly established. Many other parameters such as root function, age,

172 water retention capacity and transpiration rate in particular can affect the water flow as well as the current
173 pathway of stem-based methods (Ehosioko et al., 2020).

174 Peruzzo et al. (2020) hypothesize that drought stress can also reduce electrical current leakage wherein the
175 current exiting the plant root at the proximal part is decreased, particularly for woody species. Furthermore,
176 as expected, the frequency of the injected current plays an important role in the capacitance measured. At
177 high frequencies, both the longitudinal conductivity and radial conductivity increase (Mancuso 2012;
178 Ehosioko et al. 2020), which can also cause current leakage problems (Gu et al., 2021). The measure of
179 plant responses over multiple frequencies, a method called Electrical Impedance Spectroscopy (EIS) is more
180 time-consuming but more informative since different polarisation processes can manifest themselves in the
181 signal (Ehosioko et al., 2020). The contrast of electrical resistivities between soil and roots plays a
182 fundamental role as reported e.g. by Cseresnyés et al. (2020). Gu et al. (2021) stated that the potential to
183 directly quantify root traits under dry conditions is higher than under wet conditions and interpreted this as
184 a result of the fact that the root electrical longitudinal conductivity is higher than that of the soil under dry
185 conditions. The instrumentation and acquisition schemes used for impedance are also questionable and the
186 optimal experimental setup of measurement remains to be determined (Postic and Doussan, 2016). The
187 number and the position of the stem and the return electrodes are a cause of uncertainties (electrode contact
188 resistance, etc.). Peruzzo et al. (2021), in a three channels experiment, were able to provide direct access to
189 the response of stem and soil, which ultimately allowed the decoupling of the root response. Evidence
190 showed the presence of current leakage in herbaceous root systems, a significant contribution from plant
191 stem, and a minor impact from the soil.

192 Gu et al. (2021) stated that in addition to the traditional regression model used for predicting root traits using
193 the impedance method, a forward model would help to illustrate the importance of these different factors. In
194 order to cope with the main drawbacks of the impedance methods, we propose the so-called Electrical
195 Current Imaging (ECI) method, a physically based approach based on recovering the current density
196 distribution instead of simply calculating the total resistance/capacitance. This method is also referred to as

197 mise-à-la-masse (MALM) in the applied geophysics literature. The current imaging methods hold some
198 promise to offer a first set of evidence about the current pathways: This is a popular technique adopted e.g.
199 by the neurosciences community, where the current density in the human brain correlates with diverse
200 patterns of neural activity (Kamarajan et al., 2015). Peruzzo et al. (2020) applied it for plant roots imaging
201 with relative success, as the authors stated that all the current leaks at the plant's proximal part i.e. at the
202 shallowest contact of the plant stem with the soil. For the ECI approach, the Poisson's equation serves as a
203 physical model for the electrical current flow. As current flow is modulated by the conductivity of the soil,
204 the ECI approach is always combined with ERT in order to recover of the soil resistivity distribution.

205 **1.2. Study aims and assumptions**

206
207 The aim of this study is twofold:

208 (i) we aim at showing the correlation between the current path through the root system and the active root
209 zones. This assumption is based on the notion that soil and root hydraulic conductances are positively
210 associated with electrical conductances.

211 (ii) we want to investigate how the soil water content affects the current path.

212 For this, we rely on the following assumptions:

213 - changes in soil water content measured by ERT are a relevant spatial proxy of root activity and can be
214 used as an indicator of the actual plant transpiration by correlating them with variations of the total rhizotron
215 measured weight.

216 - During the implementation of root-zone limited water availability, when a portion of the root system in
217 the dry zone becomes deactivated, injected current in the stem tends to preferentially propagate towards the
218 side where the root system is irrigated.

219

220 **2. Material and methods**

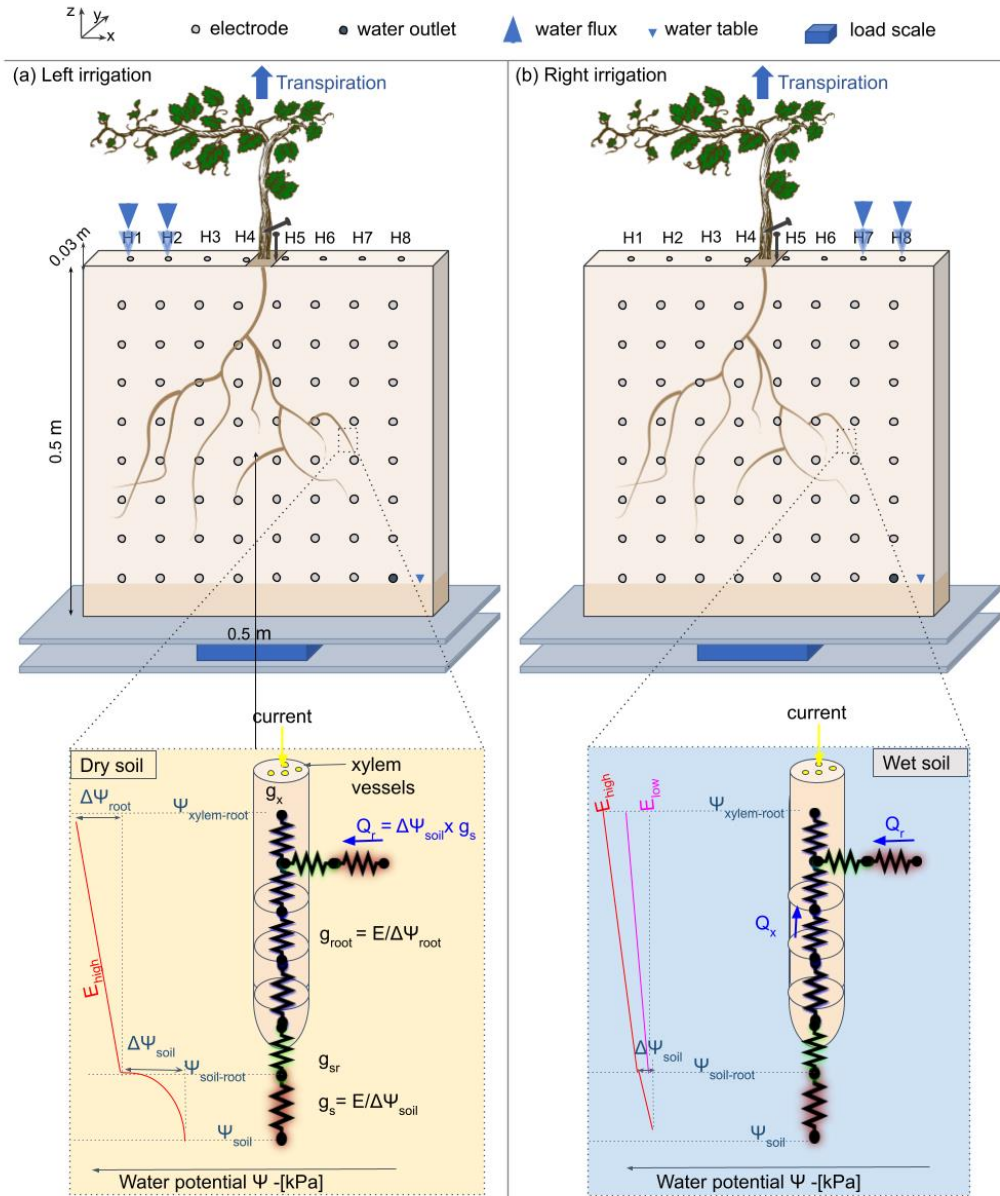
221

222 **2.1. Experimental setup**

223 **2.1.1. Rhizotron**

224 The experiment was conducted using a rhizotron 50 cm wide, 50 cm high, and 3 cm thick, with a
225 transparent screening face. The front of the rhizotron was equipped with 64 stainless steel electrodes
226 with 4 mm diameter which did not extend into the rhizotron's inner volume (Fig. 1). An additional
227 line on the top surface of the rhizotron was composed of 8 electrodes inserted to 1 cm depth. A
228 growth lamp was installed above the rhizotron and turned on during daylight hours (from 7 am to
229 7 pm). The rhizotron was closed on all sides and watertight, with only 8 small holes used for the
230 irrigation at the surface and the central hole where the plant is placed. We considered the surface
231 of these holes to be sufficiently small to neglect the possible effect of evaporation through them.
232 An outlet point was placed on the bottom right side ($z=5\text{cm}$) and the rhizotron was always saturated
233 below this point. In the course of the experiment (after the growing period) no water discharge was
234 observed through the outlet point.

235



236
 237
 238
 239
 240
 241
 242
 243
 244
 245
 246
 247

Figure 1: Conceptual figure showing the position of the plant in the rhizotron. The water input was done alternatively from left (a) to right (b) via small holes on the top of the rhizotron (H1 to H8). The roots are free to grow on both sides of the rhizotron. The circles on the screening face show the locations of the electrodes. Two additional electrodes (needles) are used for the ECI, one for the stem injection and the other for the control soil injection next to the stem. The rhizotron is weighted by a central point load scale (PC60-30KG-C3, Flintec) mounted between two support plates in plexiglass. The line below describes the state of the art of hydraulic conductivity at a single root and the distinction between dry (c) and wet (d) soil. The figure draws inspiration from the electrical circuit analogy of RWU (Root Water Uptake) proposed in previous works (Doussan et al., 1999, Manoli et al., 2014 and Couvreur et al., 2012). In a recent article, Cai et al. (2022) schematized the gradient of potential ψ_{soil} , $\psi_{\text{soil-root}}$ and ψ_{root} , along with the corresponding hydraulic conductances of the soil, the soil-root interface, and the root (represented as g_s , g_{sr} , and g_r , respectively), in response to high or low transpiration demand (E). Note that the soil-root interface and the xylem cell interfaces are seats of current polarization due to the formation of the Electrical Double Layer (EDL) well described in Tsukanov and

Schwartz (2021).

2.1.2. Plant treatment

At the initial stage of the experiment, we used a *Vitis Vinifera* cutting with a pre-developed root system (rooted cutting var. Merlot) was used. The cutting was grown in hydroponic solution (modified Hoagland medium) for 4 months before being transferred into the rhizotron. This was followed by a growing period of 5 weeks with irrigation applied over the whole width of the rhizotron every 3 days. The vine was then irrigated with a nutrient solution (see Table 1) following a PRD protocol.

2.1.3. Soil type

The experiment was conducted in a sand-peat mixture (50-50 m/m%). The applied sand was high-purity quartz sand ($\text{SiO}_2 = 99\%$) of grain size comprised between 0.1-0.6 mm and the peat was a normal commercial acidic sphagnum peat. During the course of the experiment, the soil was stable through time with very low compaction (1 cm) observed at the end of the experiment (already observed by Doussan & Garrigues, (2019) for soil with a lower density than 1.5-1.6 g/cm^3). The sand-peat mixture was chosen as a compromise between water retention and drainage. We estimated the porosity at the beginning of the experiment as equal to 55% using the ratio of water weight after saturation to the total volume of the rhizotron.

2.1.4. Irrigation schedule

We controlled the water supply for each irrigation event based on the data obtained from the scale, ensuring that the plant received 75% of the measured transpiration accumulated since the last irrigation cycle. For each cycle, the wetting side changed (from left to right). Note that in this experiment, we did not consider a physical barrier to separate the two sides of the rhizotrons to a split-roots configuration as is the case for other PRD experiments conducted in the laboratory

273 (Martin-Vertedor and Dodd, 2011; Sartoni et al., 2015). In general, the use of physical barriers in
 274 Partial Root Zone Drying (PRD) experiments is not always a standard aspect of the setup.

275 Table 1 describes all cycles conducted from May 13th to July 12th 2022:

- 276 - The goal of Cycle number 0 was to ensure plant adaptation and growth after
 277 transplantation.
- 278 - Cycle numbers 1 to 3 aimed at starting the PRD irrigation with half of the rhizotron volume
 279 irrigated; i.e. we irrigated the side through a total of four holes out of eight (see Fig. 1).
- 280 - From cycle number 4 to 10, we restricted the water input only to the two left/right most
 281 holes.
- 282 - Between cycles 4 and 5, we added intermediate irrigation on the full length of the
 283 rhizotron.

284 For the irrigation, we used a nutrient solution (modified Hoagland) (Hoagland and Arnon, 1950)
 285 having an electrical conductivity equal to $2470 \pm 5 \mu\text{S/cm}$ (at $\sim 25^\circ\text{C}$), except for cycle 3 where tap
 286 water was used ($560 \mu\text{S/cm}$).

287

Date (YYYY-mm-dd HH:MM)	Hole (H) location (c.f. Fig. 1)	Quantity (mL)*	Cycle nb
2022-05-13 16:25	All		0
2022-05-19 17:00	H1;H2;H3;H4	200	1
2022-05-25 14:30	H5;H6;H7;H8	260	2
2022-06-01 15:50	H1;H2;H3;H4	290	3
2022-06-08 11:50	H7;H8	305	4
2022-06-10	All	60	- (3bis)
2022-06-15 17:25	H1;H2	350	5
2022-06-22 16:45	H7;H8	375	6
2022-06-29 13:45	H1;H2	386	7
2022-07-05 18:10	H7;H8	431	8
2022-07-11 13:15	H1;H2	431	9
2022-07-12 16:00	H1-H8	200	-

288

289 **Table 1: Irrigation log, indicating the date, the location where the water was input and the**
290 **corresponding cycle number considered in the results. Colors correspond to the side used for the**
291 **irrigation, green is on the left side while orange is on the right side. * Quantity in total distributed over**
292 **all the holes.**

293 2.2. Electrical Resistivity Tomography

294 Electrical Resistivity Tomography consists in reconstructing the subsoil ER using an array of electrodes
295 (Binley and Slater, 2020). In this study, a total of 72 stainless steel electrodes were used, 64 electrodes
296 formed a grid, 5 cm spaced, covering the screening face of the rhizotron, and an additional line of 8 electrodes
297 was posed at the top surface. Electrodes are needles 4 mm in diameter and 80 mm in length, but only their
298 tip is in contact with the soil. ERT involves the measurement of transfer resistances following a sequence
299 describing a combination of varying injections (AB) and potential (MN) pairs of the electrodes. We used a
300 custom sequence composed of 4968 quadrupoles including the reciprocals (e.g. Parsekian et al., 2017), and
301 the measurement were conducted using a Syscal Pro (Iris Instrument) resistivity meter., The sequence was
302 optimized over the ten physical channels of the instrument in order to reduce the acquisition time to
303 approximately 30 min. The data acquisition parameters were constant along the monitoring, with a minimum
304 required V_p of 50 mV, a maximum injection voltage V_{AB} of 50 V, and a number of 3-6 stacks with the on-
305 time fixed to 250 ms each.

306 2.3. Electrical Current Imaging

307 The electrical current imaging (or Mise-à-la-masse) method was logistically similar to ERT. The sequence
308 nevertheless varies, as the pairs of injection electrodes were kept constant with the positive pole (+I)
309 electrode located on the stem, and the return (-I) electrode located in the bottom right of the rhizotron. The
310 potential electrodes pairs (MN) vary according to a custom sequence. For the stem current stimulation, we
311 inserted a small stainless steel needle (2 cm, 1 mm diameter) into the plant stem at 5 cm from the grafted
312 point. The needle was inserted all the way to the centre of the stem (Fig. 1). Before each measurement, we
313 added a few drops of water to the stem needle in order to reduce the stem contact resistance (to values

314 between 41 and 66 k Ω). The current was guided to the root system via the stem and then released into the
315 soil.

316 As the effect of the stem contact resistance affects the measured voltage, a control soil injection was
317 systematically made. In that case, the current was injected into the soil close to the plant (Fig. 1). A
318 qualitative comparison between the control soil injection and the stem injection plant could be made to
319 discriminate the effect of roots. Furthermore, soil control injection served as a visual calibration for the
320 inversion of the current source knowing that the injection is punctual and occurs at a known position.

322 **2.4. Weight monitoring for the estimation of transpiration**

323 In order to track the weight changes due to the transpiration of the plant, the rhizotron was equipped with a
324 single point load cell (PC60-30KG-C3, Flintec), mounted between two plates in plexiglass supporting the
325 rhizotron (Fig. 1). The data were logged with a sampling rate of 5 min using the weight indicator DAD-
326 141.1. The total weight of the rhizotron is about 20 kg and the expected resolution according to the sensor
327 datasheet is 0.1 g. The variation due to temperature was monitored, on average in May at 22°C, and in July
328 at 25°C. To avoid sharp signal perturbation, during the irrigation and the acquisition of geophysical data the
329 logger was paused.

330 **2.5. Leaf gas exchange observations**

331 In order to monitor the physiological response of the plant during the course of the experiment, stomatal
332 conductance to water (g_{sw} [mmol H₂O m⁻² s⁻¹]) measurements were performed on vine leaves with an open
333 flow-through differential porometer (LI-600, Li-Cor Inc., Lincoln, Nebraska, USA). The stomatal
334 conductance is a measure of the density, size, and degree of opening of the stomata, therefore it can be used
335 as an indicator of plant water status (Gimenez et al., 2005). The measurements were carried out on 26 leaves
336 in the morning hours (at 10 a.m.), once (on 8th June 2022) just before irrigation (severe water stress), and
337 once (on June 16, 2022) one day after irrigation (mild to low water stress). For the tracking of the plant
338 development, the length (L) and the width (W) of every leaf were measured every 2 weeks from the

339 beginning of the growing period until the end of the experiment. From this data the total leaf area (LA) was
340 estimated according to three models: $LA1 = 0.587 (L \times W)$ (Tsialtas et al., 2008); $LA2 = -3.01 + 0.85 (L \times W)$
341 (Elsner and Jubb, 1988); $LA3 = -1.41 + 0.527W^2 + 0.254L^2$ (Elsner and Jubb, 1988).

342 **2.6. Data processing**

343 **2.6.1. Analysis of ERT data**

344 The ERT acquisition sequence was initially tested on the rhizotron filled with water of known
345 conductivity and it offered good coverage on most of the rhizotron surface with a slight decrease
346 on the sides. The soil electrode contact resistances varied over the course of the experiment between
347 5 and 20 k Ω . Data were filtered on the basis of the percentage of variations between direct and
348 reciprocal measurements. We chose to eliminate the data with reciprocal relative errors larger than
349 5%, for all the time steps. The number of rejected data varies from 9% to 39 % of the total (see
350 Table A1) with a median of 11%. Transfer resistances were inverted using the open-source code
351 ResIPy (Blanchy et al., 2020) based on the Fortran R3t code (Binley, 2015). The inversion mesh is
352 an unstructured grid composed of tetrahedra, created using Gmsh (Geuzaine and Remacle, 2009).
353 Two distinct strategies can be used: (1) individual inversion which consists of building a model of
354 resistivity at a given time, and (2) time-lapse inversion (difference inversion) where the difference
355 in resistivity is inverted between a given survey and a background survey (in this case, the
356 background survey is the previous one). In this study, we used the second approach, which allowed
357 filtering of systematic noise and highlights variations (as a percentage of differences) between two
358 times.

359 **2.6.2. Analysis of current density**

360 The mathematical formulation for the inversion of the current source density (CSD) has been
361 developed in previous studies. It consists in searching for a linear combination of Ohm's law, for a
362 series of current punctual sources (also called virtual sources) minimizing the misfit between

363 simulated and observed data. The algorithm was initially tested on the rhizotron filled with water
 364 of known electrical conductivity and a single isolated cable (see the procedure from Peruzzo et al.,
 365 2020). It is important to note that the CSD inversion relies on the knowledge of the medium
 366 conductivity (as in the Poisson's equation, the current is modulated by the electrical conductivity).
 367 Thus, we used the inverted ER values as the resistivity distribution for the forward modelling in the
 368 current density inversion. As for ERT, choices must be made on how data and models are weighted
 369 and regularised during the inversion. In this study, we run unconstrained (no prior information)
 370 inversions for all the time steps with a regularisation (smoothing using the first derivative). The
 371 numerical routine includes a “pareto” functionality wherein regularization and model-to-
 372 measurement fit are traded off to estimate the optimum regularization weight w_r . The code used for
 373 this inversion is available at <https://github.com/Peruz/icsd>.

374 **2.6.3. Calibration of petrophysical relationships**

375 In order to estimate the soil water content in the rhizotron during the experiment, we needed to
 376 adopt a suitable constitutive model, starting from the available ER measurements.

377 Archie's (1942) law (eq. 1) is a widely used empirical relationship that relates the ER (ρ) of a bulk
 378 material to its porosity (Φ), the contained fluid (water) electrical resistivity (ρ_f) and the fluid
 379 saturation (S). Archie's parameters a , m , and n are empirically derived, generally named as follows:
 380 a is the tortuosity factor, m is the cementation exponent and n is the saturation exponent.

$$\rho = a\rho_f\phi^{-m}S^{-n} \quad (1)$$

381 We calibrated these parameters experimentally, as usually done, by collecting water saturation-ER
 382 values over different soil samples. The sample holder (a cylinder of 150 mm inner height and 41
 383 mm inner diameter) allows for a four-point measurement of the ER converted to apparent ER using
 384 the appropriate geometrical factor. The adopted water electrical conductivity is known and fixed
 385 (594 $\mu\text{S}/\text{cm}$ at $\sim 25^\circ\text{C}$). Porosity was assumed to be equal to 0.55, which is the same of the soil

386 mixture in the rhizotron. The sample was initially saturated to field capacity and progressively
387 desaturated. The field capacity was estimated by gravimetric method approximately at 40% of
388 volumetric water content (m^3/m^3). In total, 6 measurements were collected at respectively 40, 33.6,
389 29.7, 28.2, 25.2, 22.4% of volumetric water content (m^3/m^3). The obtained data are fitted with a
390 least square optimization (using the Scipy library by Virtanen et al., 2020). Here we assume a
391 equal to 1 (consistent with the theoretical value), while the exponents m and n are bounded during
392 the optimization process to respectively [1.3-2.5] and [1 - 3]. With a coefficient of determination
393 R^2 of 0.97 (figure not shown), we obtained values of 1.9 and 1.2 respectively for m and n .

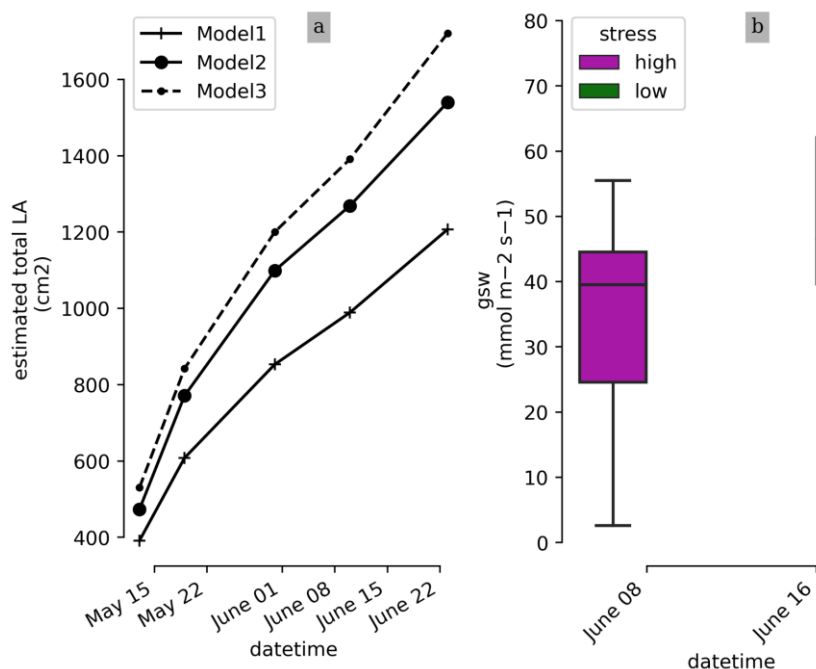
394 **3. Results**

395 **3.1. Physiological response**

396 Photographs of the plant at the beginning and at the end of the experiment show the increment of leaf area
397 extension of the upper part of the plant. The weekly measurements show a linear trend with time of the
398 estimated total LA (cm^2) whichever the model used (Fig. 2). At the end of the experiment water stress
399 symptoms were visible on some leaves.

400 As for the root system, the depth variations could not be precisely assessed during the course of the
401 experiment. We observed that: (i) roots reached the bottom part of the rhizotron; (ii) spread all over the
402 rhizotron with a network of primary, secondary, and root hairs without any given architecture (some roots
403 grew vertically, others in diagonals); (iii) the roots kept a white appearance with apparently no lignification
404 even for the largest roots ($\geq 3\text{mm}$).

405



406
407 **Figure 2: (a) Time evolution of the estimated total leaf surface area (LA) for three different model estimators. (b) leaf stomatal**
408 **conductance (High and low stress distributions are significantly different with a T-test p-value = $4.3 \cdot 10^{-3}$)**

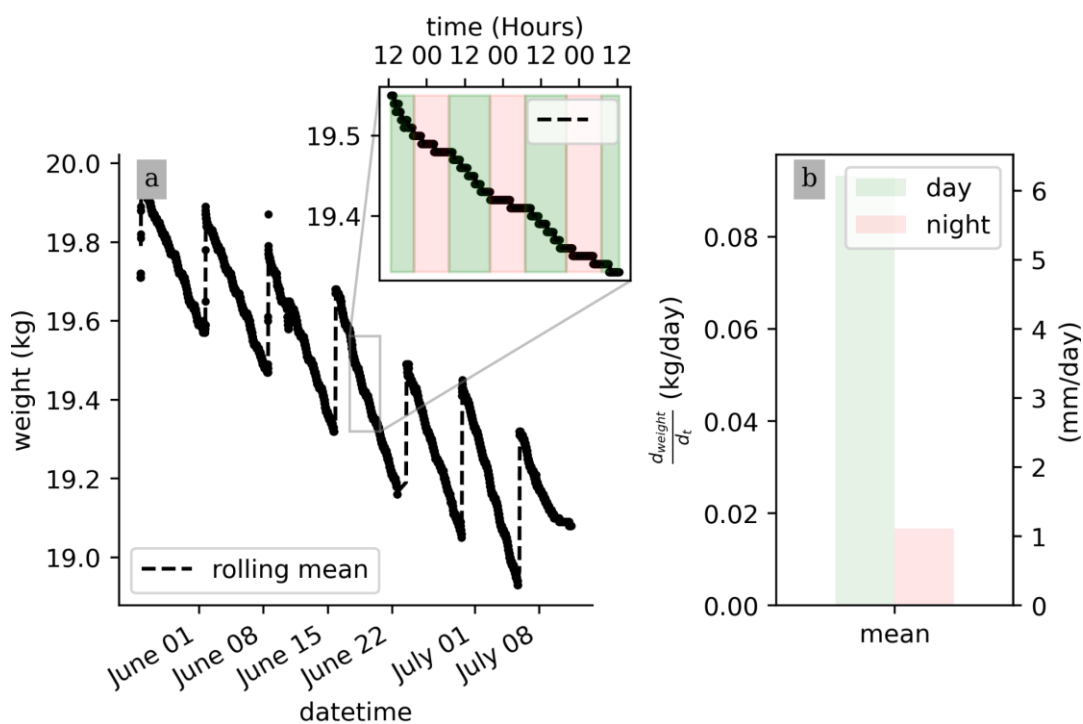
409
410 The measurements shown come from the 26 leaves (c.f section 2.5) and indicate that the plant is under high
411 water stress at the end of the irrigation cycle (one week after the last partial irrigation, on June 8,2022), and
412 under lower water stress one day after irrigation (on June 16, 2022). The mean, min, and max values of the
413 stomatal conductance (g_{sw}) values are 37.8; 23.3; 55.5 $\text{mmol m}^{-2} \text{s}^{-1}$ before irrigation, respectively, and
414 50.6; 18.9; 78.1 $\text{mmol m}^{-2} \text{s}^{-1}$ after irrigation, respectively. The result of the T-test shows that their mean
415 values are significantly different (p-value = $4.3 \cdot 10^{-3}$).

417 3.2. Transpiration rate

418 No pre-processing of the raw data is needed for their interpretation. Fig.3 shows that, on average, during a
419 PRD cycle (about one week), 0.5 kg of water transpired. Also, the weight data show that the total weight is
420 decreasing from one cycle to the next, as expected, due to the PRD protocol. Although the total water content

421 is decreasing, the transpiration rate (slope of the weight variations) remains constant for each cycle. At the
 422 very end of the experiment from July 9, an inflexion point is observed and the weight stops decreasing.
 423 Zooming on a shorter time window, the variation of the raw data weight clearly shows day/night patterns
 424 triggered by the hours when the light is switched on/off. On average, the water lost during the day is nearly
 425 20 times more than during the night (0.09 kg/day against 0.005 kg/night). Note that there is no distinction
 426 between the hours of the day (due to artificial lighting).

427
 428
 429



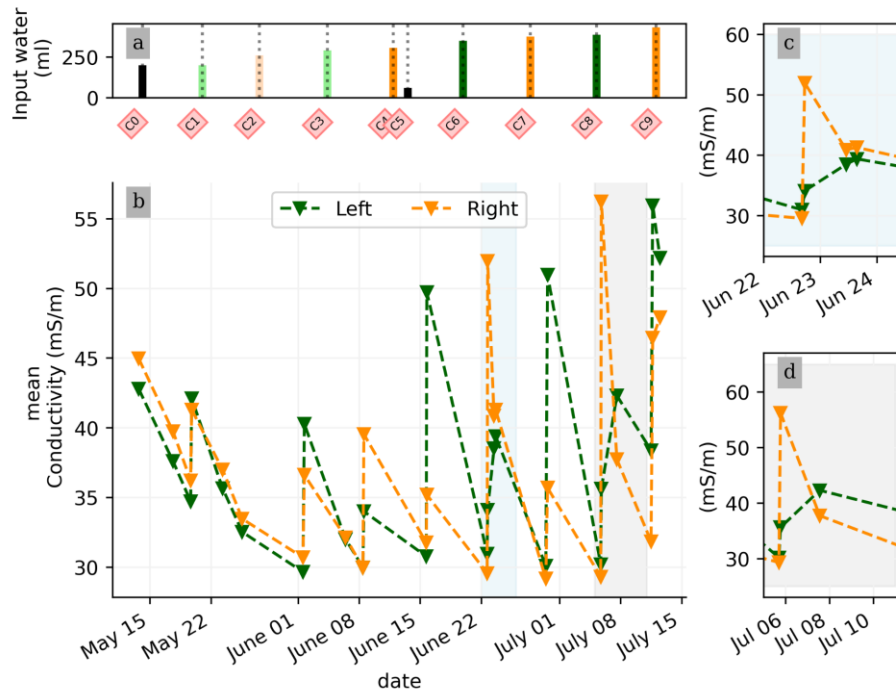
430
 431
 432
 433

Figure 3: Raw scale data collected over the course of the experiment (a) and a zoom on the week of June 20 to 25, where day and night periods are respectively highlighted by the green and red shaded areas. (b) Calculated daily mean transpiration (d_{weight}/d_t) during the day (green) and night (pink) periods.

434
435
436
437
438
439
440
441
442
443
444
445
446
447
448
449
450
451

3.3. Time-lapse ERT

In general, the ERT data quality is very good with a small percentage of total measurements exceeding a reciprocal noise level of 5% (see Fig. A1 to A11) and with each inversion resolved within 2/3 iterations. Figure 4 shows the trend for the PRD cycles (from cycles 0 to 9) for the mean average electrical conductivity (in mS/m) for both the wet and dry sides of the rhizotron, taken as an average of each half of the ERT inversion mesh elements. When PRD is applied over only two holes (from cycle 3) the irrigated side shows a clear increase in electrical conductivity. To a much lower degree, the dry side is also affected by the water input, likely due to water redistribution during drainage. When available, the temporal dynamics between two irrigations show that the conductivity is decreasing rapidly on the irrigated side during the 2 first consecutive days and more slowly afterwards (cycles C5/6 and C7/8 respectively; Fig. 4c and Fig. 4d). As some water infiltrates also on the dry side, we also observe an increase in conductivity in it. At the end of each cycle (the cycle length is about 7 days), the rhizotron returns to the equilibrium condition, with a more homogeneous and stable average conductivity equal to 30 mS/m (mean of the dry and wet sides). This is generally true for all times, except at the end of the experiment, cycles 7 and 8, when the two sides are in different conditions.



452

453 **Figure 4: (a) Evolution of the quantity (in ml) of water input, spatially distributed with alternating between left (green) and right**
 454 **(orange) before and during the PRD irrigation. (b) Evolution of the mean conductivity (mS/m) average on each side, markers show**
 455 **the acquisition time. (c) and (d) are inset zooms showing changes before and just after the irrigation event.**

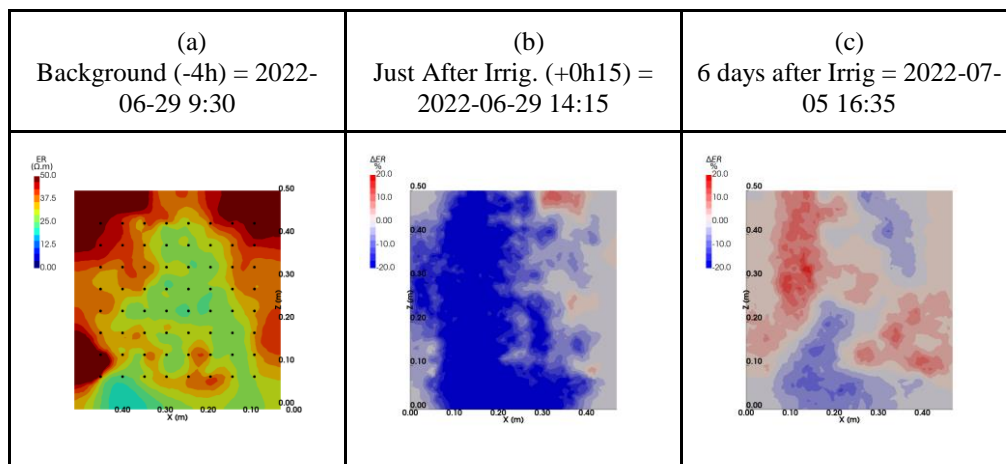
456

457 We selected a time window between 29 June and 5 July showing the spatial variations of the ER before and
 458 after an irrigation event (Fig. 5). Before the irrigation, the top and left-most and right-most boundaries of the
 459 rhizotron exhibit higher ER (50 Ohm.m) than the central part (25 Ohm.m). One hour afterwards (+ 1H) the
 460 ER of the left irrigated side had dropped by 20% (estimated from the averaged values spanning from the
 461 middle of the rhizotron to the left boundary) .

462 All time-lapse inversions before/after irrigation are shown in Appendix A, including before the PRD. They
 463 all show that a decrease in ER is associated with irrigation patterns while an increase in ER has a more
 464 complex spatio-temporal dynamics, not systematically associated with irrigation patterns. Changes in ER
 465 after six days (day +6) show that RWU effects are not limited to the irrigated part since the increase of
 466 resistivity was also observed on the dry part. Note from a visual inspection of the rhizotron a water table
 467 forms at 0.4 m where the soil is saturated. This saturated zone level is not affected by the irrigation as no

468
469
470

increase after irrigation, and no decrease by the end of the irrigation cycles are visible. We assume that most of the water fluxes were connected to the unsaturated part.



471

472 **Figure 5: Spatial distribution of the resistivity (in Ωm) and changes (in %) in ER obtained by a time-lapse inversion between cycle**
473 **6 and 7 following partial left irrigation of the rhizotron. Time steps correspond to measurements before (a), 15 minutes (b) and 6**
474 **days (c) after irrigation started.**

475

476 3.4. Time-lapse ECI

477

478

479

480

481

482

483

484

485

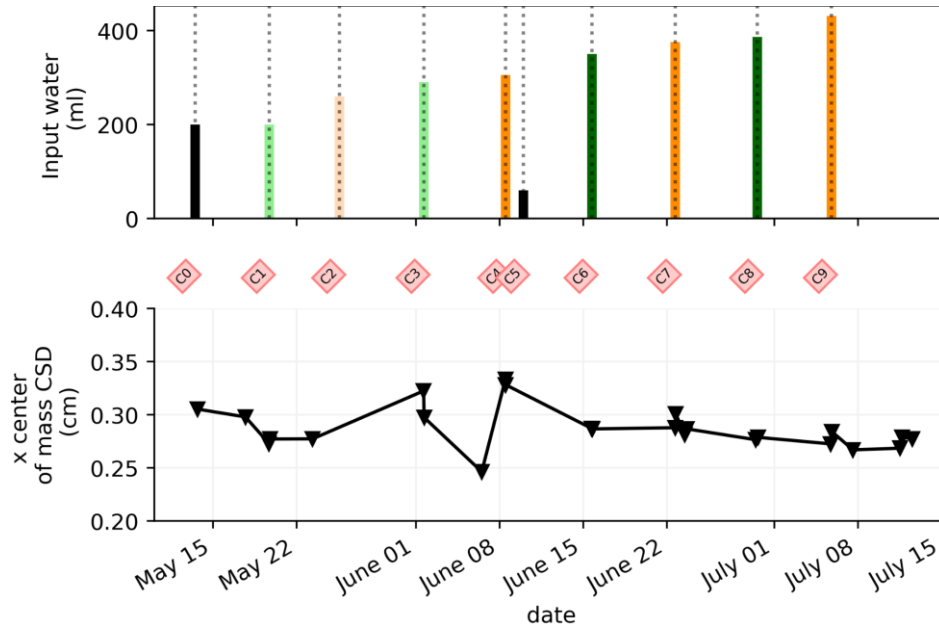
486

487

Figure 6 shows the trend of the horizontal location (x coordinate) of the centre of mass of current density during the PRD cycles (from -1 to 8), after the alternative wetting events on the left and right sides of the rhizotron. Considering the modulation of current by soil electrical resistivity (ER), any bias in ER could introduce errors in forward current source imaging and, consequently, affect the positioning of the current source. The soil CSD is not shown as it is always pinpointed to the location of the injection electrode whatever the irrigation pattern, as expected (Figure 7abc). This result confirms the quality of the estimated ER background values used for the ECI forward model. For the stem injection, the centre of mass of the current source density is distributed equally from left to right except for cycle 4 when most of the current is located on the left (see Fig. B1 to B4). Conversely to ER variations, the irrigation pattern does not significantly affect the current density distribution. The same applies to the temporal dynamics between two

488
489
490

irrigations where the current density centre of mass is stable and distributed equally on both sides, as shown in Fig. 7. All the time-lapse inversion results of current density for the soil and the stem injection are shown in Appendix B.



491
492
493
494
495

Figure 6: (a) Evolution of the quantity (in mL) of water input spatially distributed alternatively between left (green) and right (orange) during the PRD irrigation. (b) Evolution of the centre of mass (in the x direction) of the current density, while cross markers show the acquisition times. Cycle 7 and 8 windows were selected for the MALM time-lapse spatial analysis (Figure 7).

Background = 2022-06-29 (cycle 7)	Just after irrigation (H+1) = 2022-06-29 14:15	Day + 6 = 2022-07-05 16:35
a (soil control, 10:24)	b (soil control, 15:02)	c (soil control, 17:55)
d (stem, 10:14)	e (stem, 14:50)	f (stem, 17:15)

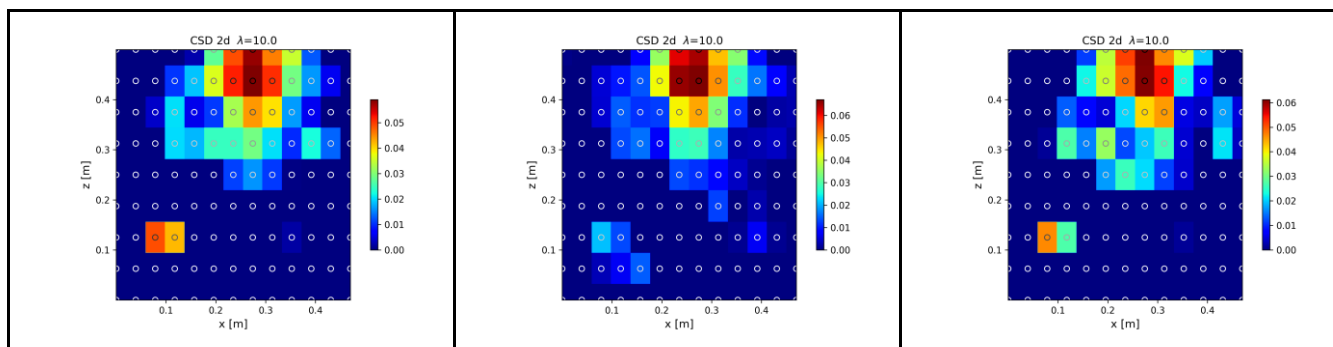


Figure 7: Spatial distribution of the CSD between cycles 7 and 8 following partial (right) irrigation of the rhizotron for the soil control injection (a,b,c) and the stem injection (d,e,f). The larger spread of current sources in the stem injection (d, e, f) compared to soil control injection (a, b, c), demonstrates that the root system plays a key role in the distribution of the current source in the soil. Time steps correspond to measurement before (a,d) irrigation, one hour after irrigation (b,e), and after 6 days (c,f). The regularisation parameter wr is fixed to 10 for both cases (see section 2.6.2 for the choice of wr).

496

497

498

3.5. Correlations between soil parameters and estimated transpiration rates.

499

500

501

502

503

504

505

506

507

508

509

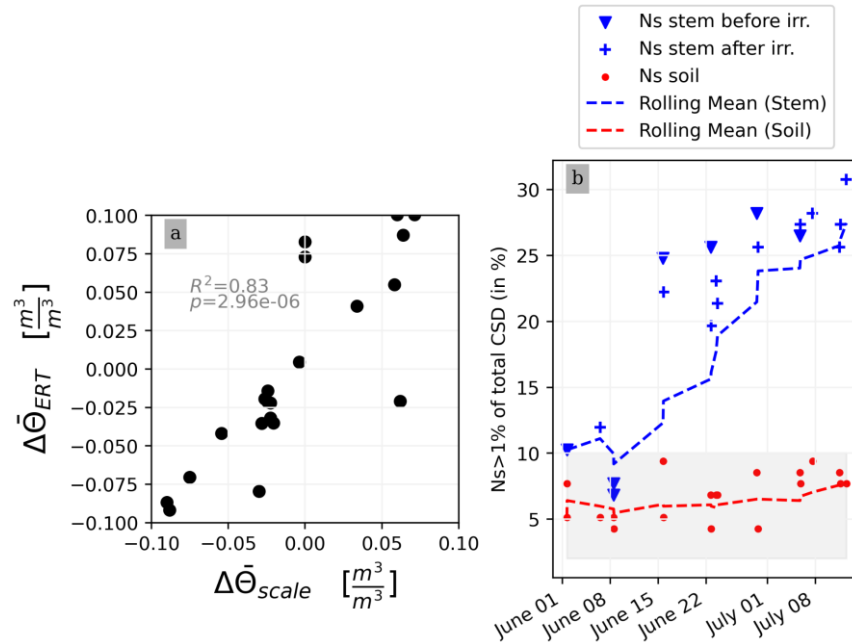
510

511

This section aims at drawing correlations between the soil parameters (ER, SWC, and CSD) and the transpiration estimated from the rhizotron weight data. We do not account for the weight variations due to the plant and root growth material (as this can be considered negligible relative to water dynamics). For each node of the mesh, ER values are translated to SWC using Archie's law with the calibrated parameters m and n (see Sect. 2.6.3). Averaging is performed on the mesh nodes falling within each side, with the middle point being defined as half of the rhizotron width, equivalent to 0.25m. To simplify, we assume that both porosity and fluid water conductivity are homogeneous in space and time (i.e no mixing between the tap water used for cycle 3 and the nutrient solution for all the other times). The maximum SWC observed after irrigation is about $0.42 \text{ m}^3/\text{m}^3$ (figure not shown). The minimum SWC of about $0.25 \text{ m}^3/\text{m}^3$ is repeatedly observed (see Fig. C1) just before each irrigation, meaning that the driest times are below field capacity conditions (estimated at $0.4 \text{ m}^3/\text{m}^3$). By examining the fluctuations in weight, one can calculate the corresponding changes in spatially averaged water content. Figure 8a illustrates a linear trend ($R^2=0.83$ and $p=2.96e-6$) between the inferred water content variations from the scale and those obtained from ERT (after Archie

512
513
514

transformation). The most significant negative changes in averaged water content are attributable to the triggered irrigation, leading to a $\Delta\bar{\Theta}$ (change in water content) of -0.1. Conversely, positive changes primarily result from transpiration, with a maximum value located at +0.1.



515

516 **Figure 8: (a) Changes in water content calculated from weight changes related to the changes in water content calculated from the**
 517 **ERT measurements. (b) relationship between the number of the current sources (Ns) carrying at least 1% of the total density**
 518 **(A.m-2) with respect to the time of the experiment. CSD results are obtained after inversion with a regularisation parameter wr of**
 519 **10. Cases of the stem before cycle 3 (grey), after cycle 3 (black) and the soil (blue) injections. All cycles are considered.**
 520
 521

522

523

524

Figure 8b shows the relationship between the variation of the percentage of the current sources carrying at least 1% of the total density (Ns1) used as an estimator for current density dispersion with respect to the datetime of the experiment. For the soil injection (red dots), Ns1 is relatively constant between 5 to 10% of the total number of possible injection nodes (grey area). For the stem injections, Ns1 increases over the course of the experiment. From June 1st to July 8th, the Ns1 triple. There is no distinction between Ns1 measured before (triangle point) and after (crossed points) irrigation.

529

530 **4. Discussion**531 **4.1. Validity of ERT and ECI in demonstrating the effects of the alternating irrigation scheme**

532 Our first assumption was that the variations in ER (or in SWC inferred from the ER) are relevant as a proxy
533 of root activity. Its validity has been checked against direct observation using the variations of weights
534 measured from the scale data used as an indicator of plant transpiration. On average, in our experiment, the
535 plant maintained high rates of transpiration to about 6 mm/day for each cycle except for the last cycle
536 (number 9) where a decline was observed (Fig. 3). This range is in line with another rhizotron experiment
537 where narrow-leaf lupin plants were grown: Garrigues et al. (2006) measured a mean rate of 3 mm/day. It is
538 commonly found in the scientific literature that changes in ER are associated with root activity (e.g., Michot
539 et al., 2003; Garré et al., 2011; Cassiani et al., 2015; Whalley et al., 2017). Here we had further confirmation
540 of this, with a significant correlation between ER changes and gravimetric soil moisture changes (derived
541 from the load cell) (Fig. 8). The leaf stomatal conductance and visual observation of plant above- and below-
542 ground material growth were additional ancillary data to interpret the general state of the plant. Our
543 observation is in line with the literature i.e. in general, low soil water content (SWC) can lead to drought
544 stress in plants, which can result in decreased leaf stomatal conductance and less transpiration, and vice-
545 versa.

546
547 A second assumption was that, when applying the alternative irrigation scheme, only one part of the root
548 system would be active and the current injected in the stem would only spread to the side where the root
549 system is irrigated. This assumption was not directly supported by the observations. Figures 6 and 7 show
550 that the influence of the irrigation pattern was negligible on the spatial distribution of the inverted CSD and
551 that the current distribution was not correlated with ER variations. It is true that active roots have higher
552 hydraulic conductivity but on the other hand, increased membrane permeability may encourages current
553 leakage into the soil. We nevertheless noticed that the CSD spatial distribution, while the rhizotron is
554 irrigated at its full length (cycles 0 to 3), was significantly different from the side irrigation cycles (Fig. B4).

555 Indeed, homogeneous irrigation without applying stress to the plant results in a very shallow current leakage.
556 Our observations potentially suggest that under conditions where soil electrical conductances are high near
557 the soil-root interface and even if there is good electrical contact between soil and roots, the distribution of
558 current source density might not be directly related to water uptake distributions. Further research is needed
559 to confirm this potential relationship.
560

561 **4.2. Effect of soil water content and transpiration demand**

562 Soil water content can affect the distribution of the current leakage by influencing the minimum resistance
563 pathways, i.e., whether roots and/or soil provide the minimum resistance to the current flow. Literature
564 reports that electrical capacitance method better estimates crop root traits under dry conditions (Gu et al.,
565 2021). In order to make a comparison with capacitance studies, we assumed that if the current distribution
566 remains unchanged (i.e. leaking into the same areas), there must be minimal changes in the electrical
567 capacitance. In this study, supposing no impact of the initial model, Fig. 9 shows that there is no apparent
568 effect of the soil water content on the current density distribution. Note that the soil water content estimated
569 is the bulk contribution of roots and soil, as only one pedophysical relationship was used, while recent studies
570 tend to show that mixed soil-root pedophysical relationships are preferable (e.g. Rao et al., 2018). Moreover,
571 considering small-scale variations around individual root segments in terms of water content and soil
572 hydraulic properties becomes crucial for a comprehensive understanding of the system.. This is clearly
573 limiting our ability to interpret the independent contribution of the soil and the roots, yet this does not limit
574 our ability to identify zones where water availability leads to root water uptake.
575

576 Based on Fig. 2 and 8b, the association between water stress and leaf development, along with transpiration
577 demand, is expected to be more prominent (and increasing during the course of the experiment rather than
578 the specific time points before and after irrigation). Indeed the fluctuations in water content during various
579 cycles, with or without stress, exhibited remarkable similarity. Both stressed and non-stressed cycles

580 experienced a drop in water content to similar low levels. Consequently, water content does not appear to
581 account for the variability in water stress. Instead, it is the increased transpiration demand over time that
582 seems to play a more significant role in driving the observed changes. At high transpiration demand, stress
583 may occur at higher soil water contents because the soil becomes limiting for the root water uptake. The
584 changes in water potential and water content in the vicinity of the soil-root interface can potentially impact
585 the electrical conductivity of the immediate soil surrounding the roots. Consequently, as the experiment
586 progressed, lower electrical conductances in the soil around the roots, potentially led to a restriction in the
587 flow of current between the root system and the soil. This, in turn, may have resulted in a more uniform
588 distribution of the electrical current source along the entire length of the root system.

591 **4.3. Possible mitigation of the PRD effect**

592 In general, a PRD irrigation experiment must comply with two criteria: (1) a minimum soil water content to
593 trigger a physiological response and, (2) a distinction between a wet and a dry side (Stoll, 2000). In our
594 experiment, the first criterion was met, but not the second. This provides an interesting piece of evidence,
595 leading to the following considerations:

- 596 (1) According to McAdam et al. (2016) and Collins et al. (2009), ABA is triggered even by mild soil
597 stress values. Consequently, plants adapt the hydraulic conductivity of their roots as well as that of
598 the soil in their vicinity through exudates (Carminati and Javaux, 2020). Results from previous
599 irrigation experiments using PRD or DI have shown that changes in stomatal conductance and shoot
600 growth are some of the major components affected (Düring et al., 1996). In our experiment, the
601 shoot growth fitted with the conventional leaf area and growth models, except at the end of the
602 experiment when signs of water stress were visible on some leaves. The magnitude of the shoot
603 growth is correlated with the number of roots. Drought may cause more inhibition of shoot growth
604 than of root growth (Sharp and Davies, 1989). Although the root system was already well developed
605 it is not possible to exclude its development as a factor influencing the CSD distribution.

- 606 (2) The spatiotemporal analysis of the ER showed that the water changes were not limited to root
607 effects. Water redistribution from dry to wet in the soil and from shoot to dry roots (Smart et al.,
608 2005, Lovisolo et al., 2016) may have occurred (Fig. A1 to A11). Additionally, even not visible
609 from the screening face, capillary rise may have taken place due to the presence of a saturated zone
610 at the bottom of the rhizotron. Due to the fact that water drained on both sides, RWU was not only
611 vertically distributed but also horizontally. The range of water content varied significantly with a
612 minimum SWC of about $0.25 \text{ m}^3/\text{m}^3$, repeatedly observed just before each irrigation meaning that
613 the driest times are below field capacity conditions (estimated at $0.4 \text{ m}^3/\text{m}^3$). Drying half of the root
614 system resulted in a reduction of the stomatal conductance (based on the mean of the distribution)
615 of the order $5 \text{ mmol m}^{-2}\text{s}^{-1}$ after a 1 week cycle. Given the stress applied, the ER changes
616 highlighted that root played a major role in the wine plant survival and evidenced strategies of
617 adaptation. Indeed, the plant was able to adjust its water uptake and redistribution zones depending
618 on the water availability, from all places, not only from the alternate irrigated areas.
- 619 (3) Finally, in order to know if the PRD conditions are met it would have been important not to neglect
620 the different states of root growth, and root renewal (because of renewal and decay) with respect to
621 the geophysical data. Nevertheless, this would have required opening and scanning the rhizotron
622 with conventional methods. Finally, we did not make a distinction between the hours of the day
623 although the changes observed for the irrigation are rapid, usually at the hourly scale, and could be
624 similar for RWU.

625 626 627 **4.4. Performance of the acquisition protocol and the processing**

628
629 We discuss here how the quality of the recovered current density models by evaluating the performance of
630 the protocol and the processing. First, it is important to note that although the ERT data quality was good

631 (very few reciprocals were rejected, see Table A1), the inverted model was not perfect and this ultimately
632 has an impact also on the ECI forward model. The algorithm has undergone testing in a rhizotron experiment
633 and has demonstrated the ability to differentiate punctual sources, even when their current contribution is as
634 low as 5% of the total current (Peruzzo et al., 2020). The CSD resolution, of course, matches the electrode
635 interspace (in this case 5cm) and the smoothness constraint does not impact the simulation of point source
636 reconstruction. We adopted an inversion without any prior information to recover the current density. Only
637 model smoothing was applied by weighting the model data by an optimal factor of 10 inferred from an L-
638 curve analysis. Similar to the ERT inversion, the CSD problem is also ill-posed. In this case, the 4-electrodes
639 setup ensures that the current will flow through the plant after injection, regardless of the contact resistance.
640 However, the accuracy of the measured data may be impacted by contact resistance, as errors in the measured
641 resistance will negatively affect the quality of ERT and CSD inversions. The impact is more pronounced on
642 CSD, as it is dependent on ERT. Lastly, because the box is relatively small and no-current-flow boundary
643 conditions (Neumann) are imposed, we may expect an effect due to the position of the return electrode where
644 the current is attracted due to the strongest gradient nearby (Mary et al., 2019b).

647 **4.5. Outlook**

648 In order to strictly correlate PRD effects with geophysical measurements, one should consider a physical
649 barrier to separate the two sides of the rhizotron to a split-roots configuration. Another option is to increase
650 the lateral size to prevent redistribution or to use a very percolating material such as glass beads, gravels or
651 coarse sands. This should be carefully considered, as the rhizotron must also be an environment where plant
652 growth is possible under “natural” conditions, and for this some water retention capacity is needed for the
653 soil. A larger drainage capacity would simplify the interpretation as no-water redistribution from one side to
654 the other can occur. Although considering a barrier is technically possible, it would require a more complex
655 inversion scheme of the ERT and ECI considering that no electrical current can flow from side to side. One

656 could also consider increasing the measurement frequency to catch processes at an hourly scale and
657 comparing day/night measurements, particularly those associated with water redistribution from the stem
658 back to the roots at night when transpiration is reduced and its effect on the water status of the roots. As we
659 have seen that most of the water changes occurred in the day consecutive to the irrigation, catching rapid
660 changes of ER would help drive a conclusion on how much ECI is connected to the active root zone. Finally,
661 in order to draw robust statistical conclusions, the experiments should be replicated for multiple plant
662 samples.

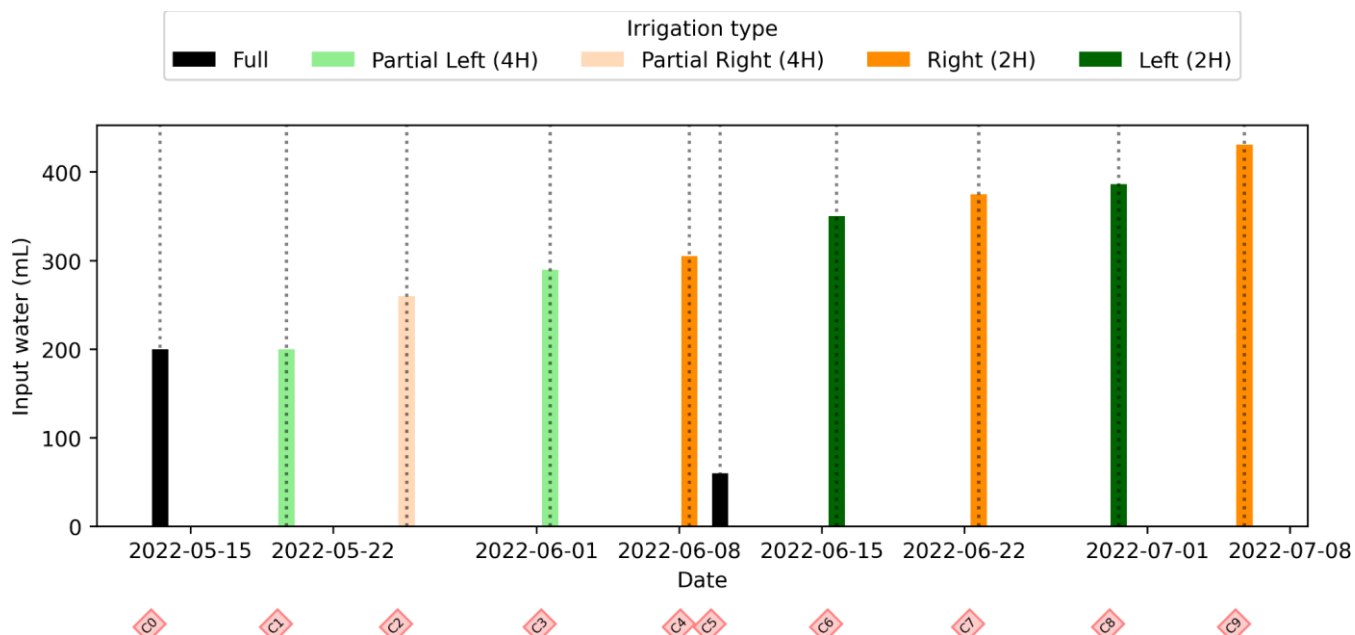
663 **5. Conclusion**

664 The study aimed at understanding the current path in the root system and active root zones using geoelectrical imaging,
665 considering soil water content and irrigation regimes. Electrical Resistivity Tomography (ERT) is sensitive to both irrigation
666 and RWU processes. The ECI model uses a physical approach to measure current density after stem stimulation. The CSD was
667 very different from the control soil injection to the stem injection but nevertheless did not correlate with PRD cycles as
668 originally expected. We demonstrate that under mild stress conditions, it is practically impossible to spatially distinguish the
669 PRD effects using the ECI. We only evidenced that the Current Source Density distribution varied during the course of the
670 experiment considering evaporative demand but without any significant relationship to the Soil Water Content changes . A
671 few aspects of the experiment would gain to be more closely studied such as the water redistribution that possibly also affects
672 current distribution. In the future, we expect to improve our understanding by coupling the geophysical experiment with an
673 unsaturated soil-plant-atmosphere model.

674 **6. Appendices**

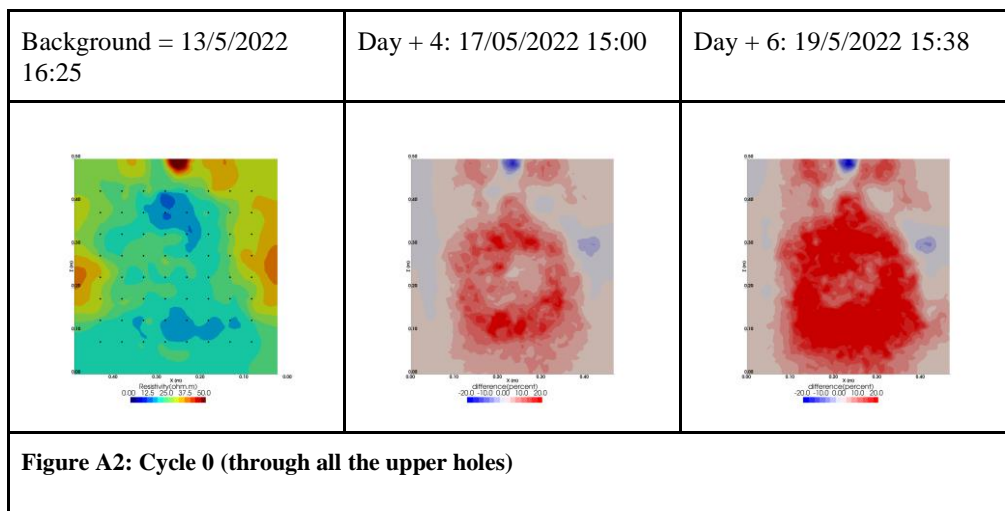
675 **Appendix A: Time-lapse ERT inversion results**

676 As we selected only one cycle in the manuscript, we report here further details about the time-lapse ERT inversion results for
677 all the cycles. The inversion procedure is equivalent to the one described in Sect. 2.6.1 of the manuscript (Data processing -
678 Analysis of the ERT data). All time-lapse inversion models are plotted with a unique scale ranging from -20 to 20% of changes.
679



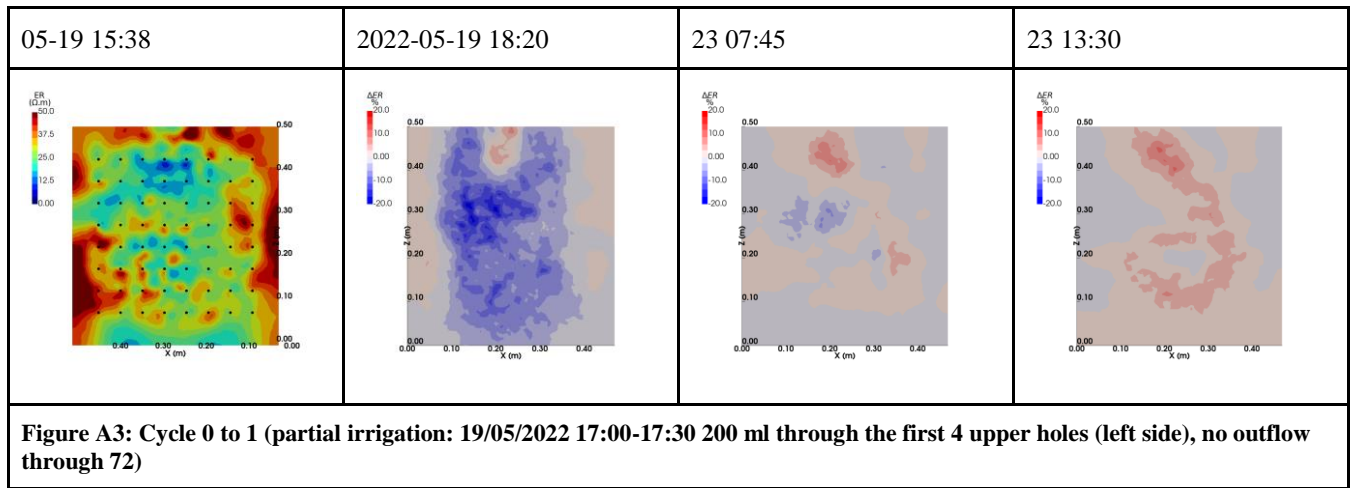
680
681
682
683
684
685
686

Figure A1: Evolution of the quantity (in mL) of water input spatially distributed with an alternate between left (green) and right (orange) during the PRD irrigation. The black bars hold for full-width irrigation (over all the holes, see fig. 1 manuscript), light green and orange bars hold for irrigation over the 4 sides of holes, and dark green/orange for 2 holes irrigation.



687
688

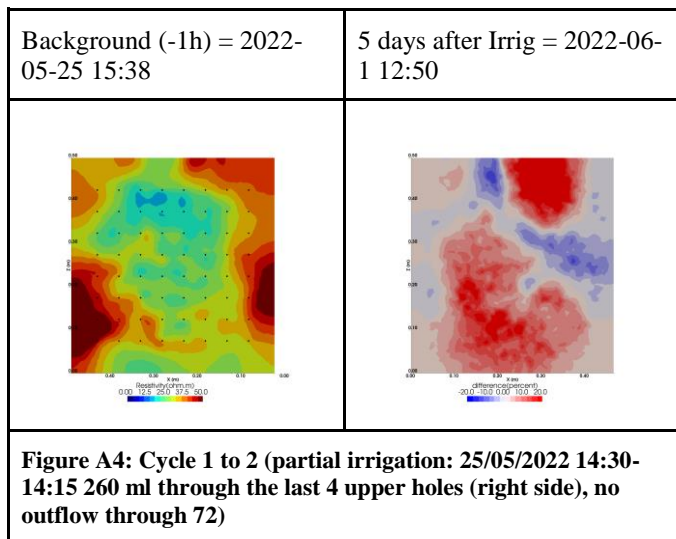
Background (-1h22) = 2022-	Just After Irrig. (+1h20) =	4 days after Irrig = 2022-05-	6 days after Irrig = 2022-05-
----------------------------	-----------------------------	-------------------------------	-------------------------------



689
690

691

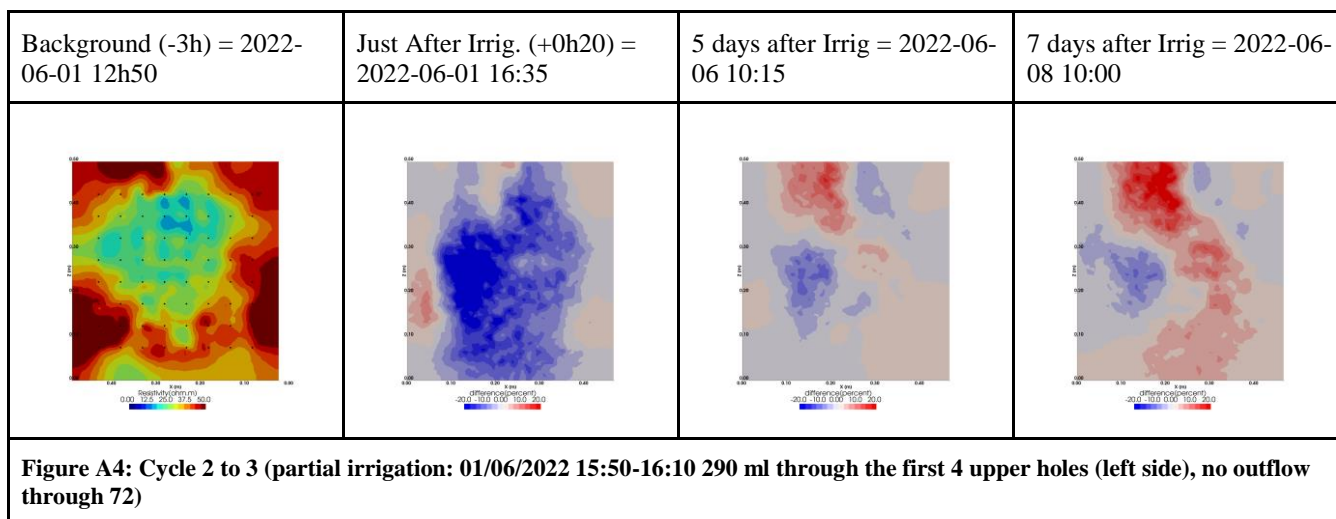
692



693

694

695



696

697

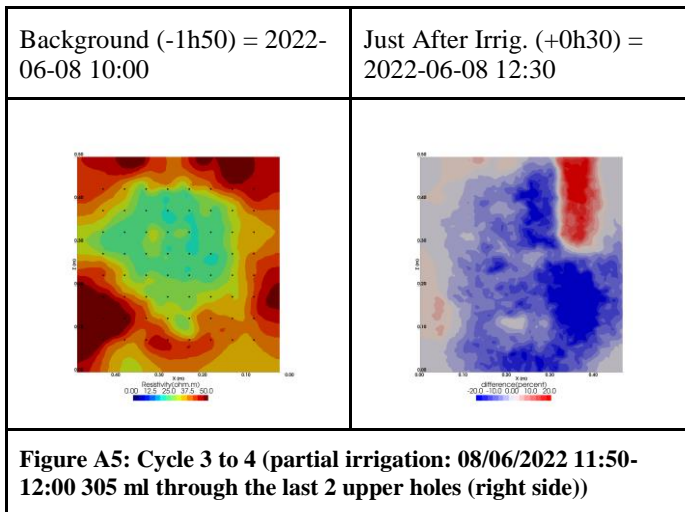
698

699

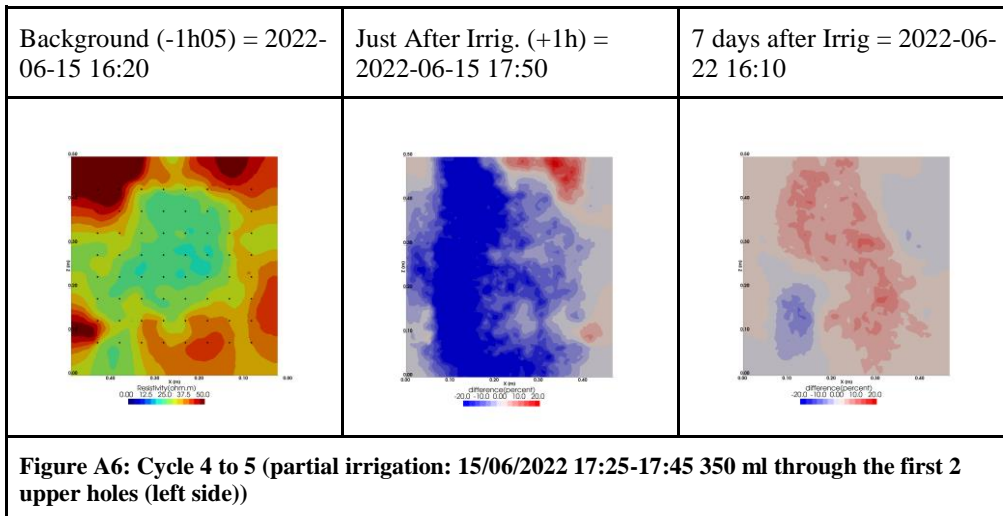
700

701

702



703



704

705

706

707

708

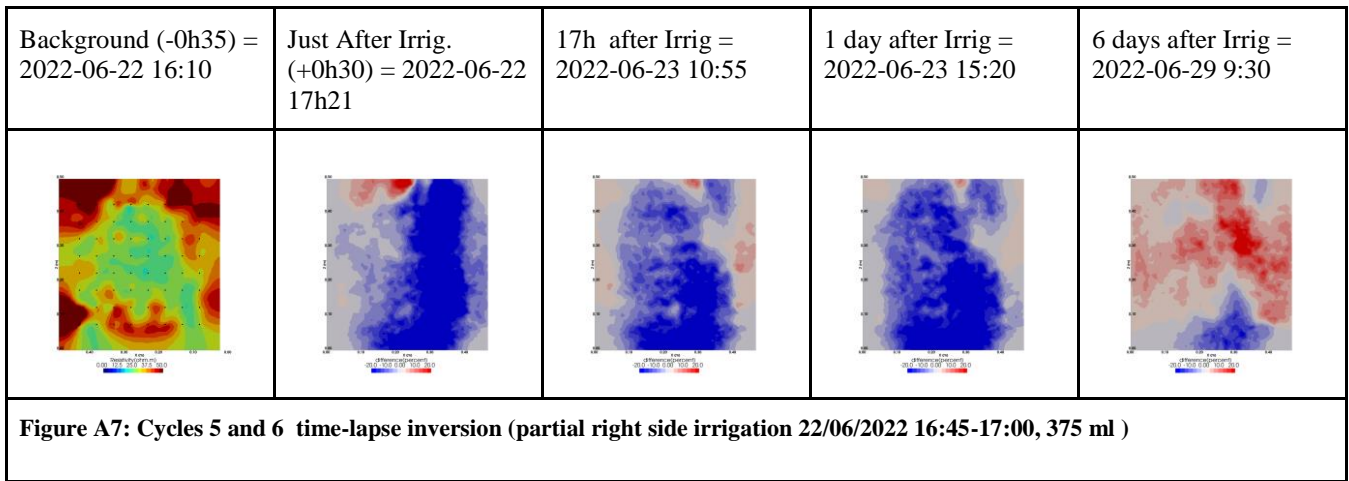
709

710

711

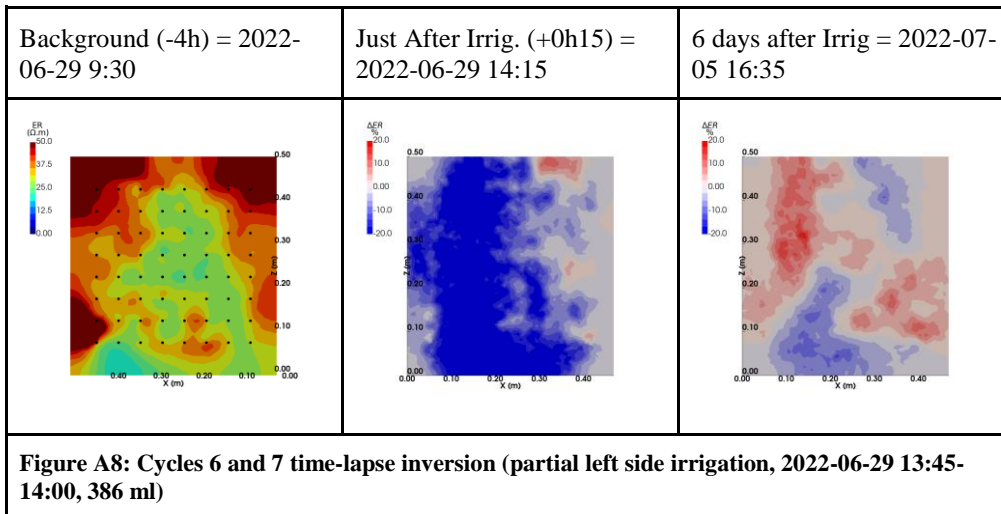
712

713



714

715



716

717

718

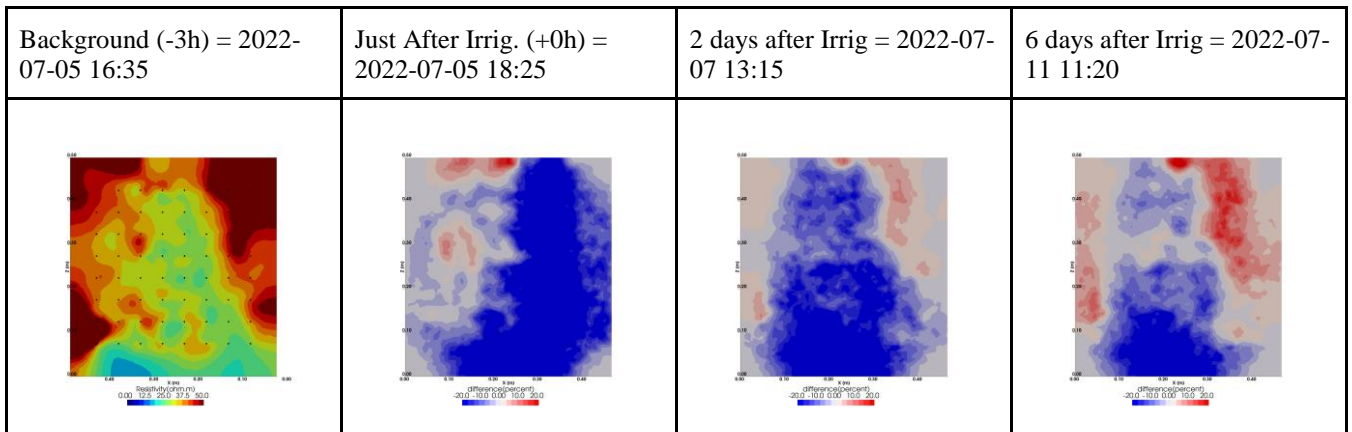


Figure A9: Cycles 7 and 8 time-lapse inversion (partial right side irrigation, 2022-07-05 18:10-18:25, 431 ml)

719
720
721

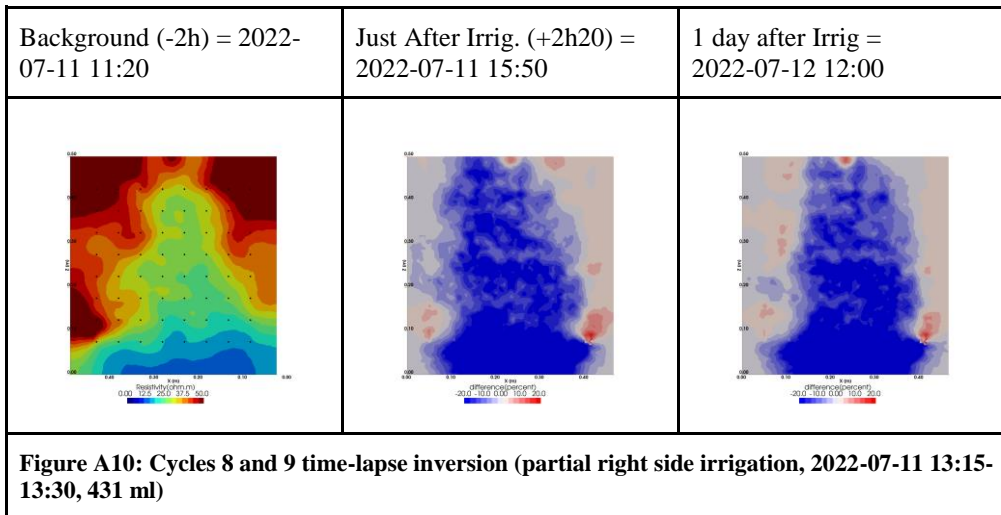


Figure A10: Cycles 8 and 9 time-lapse inversion (partial right side irrigation, 2022-07-11 13:15-13:30, 431 ml)

722
723
724
725
726
727
728
729
730

Date	RMS (%)	# measurements read (over 2484)
2022-06-01 12:50:00	1.36	2048
2022-06-01 16:35:00	1.15	1920
2022-06-06 10:15:00	1.53	2268
2022-06-08 10:00:00	1.41	2230
2022-06-08 12:30:00	1.16	2028
2022-06-15 16:20:00	1.08	2137
2022-06-15 17:50:00	1.47	1493
2022-06-22 16:10:00	1.38	2109
2022-06-22 17:21:00	1.14	1372
2022-06-23 10:55:00	1.48	2229
2022-06-23 15:20:00	1.38	2268
2022-06-29 09:30:00	1.27	2075
2022-06-29 14:15:00	2.04	2027
2022-07-05 16:35:00	1.7	2067
2022-07-05 18:25:00	1.85	980
2022-07-07 13:15:00	1.98	2225
2022-07-11 11:20:00	2.5	2093
2022-07-11 15:50:00	2.72	2238
2022-07-12 12:00:00	2.68	2255

731 **Table A1: Table summarising the final RMS and the number of data used for each individual inversion**

732

733

734

735 **Appendix B: Inversion of current density (CSD)**

736

737 As we selected only one cycle in the manuscript, we report here further details about the time-lapse CSD inversion results for
738 all the cycles. The inversion procedure is equivalent to the one described in Sect. 2.6.2 of the manuscript (Data processing -
739 Analysis of current density) and we invite the reader to refer to Peruzzo et al. (2020) for a full description of the algorithm.
740 Furthermore, we extend the analysis showing the effect of the model regularisation (smoothing). Figures B1 and B2 show the
741 current density evolution with the time respectively for the stem and the soil injection with a regularisation parameter of 1.
742 The same is for Figures B3 and B4 with a regularisation of 10.

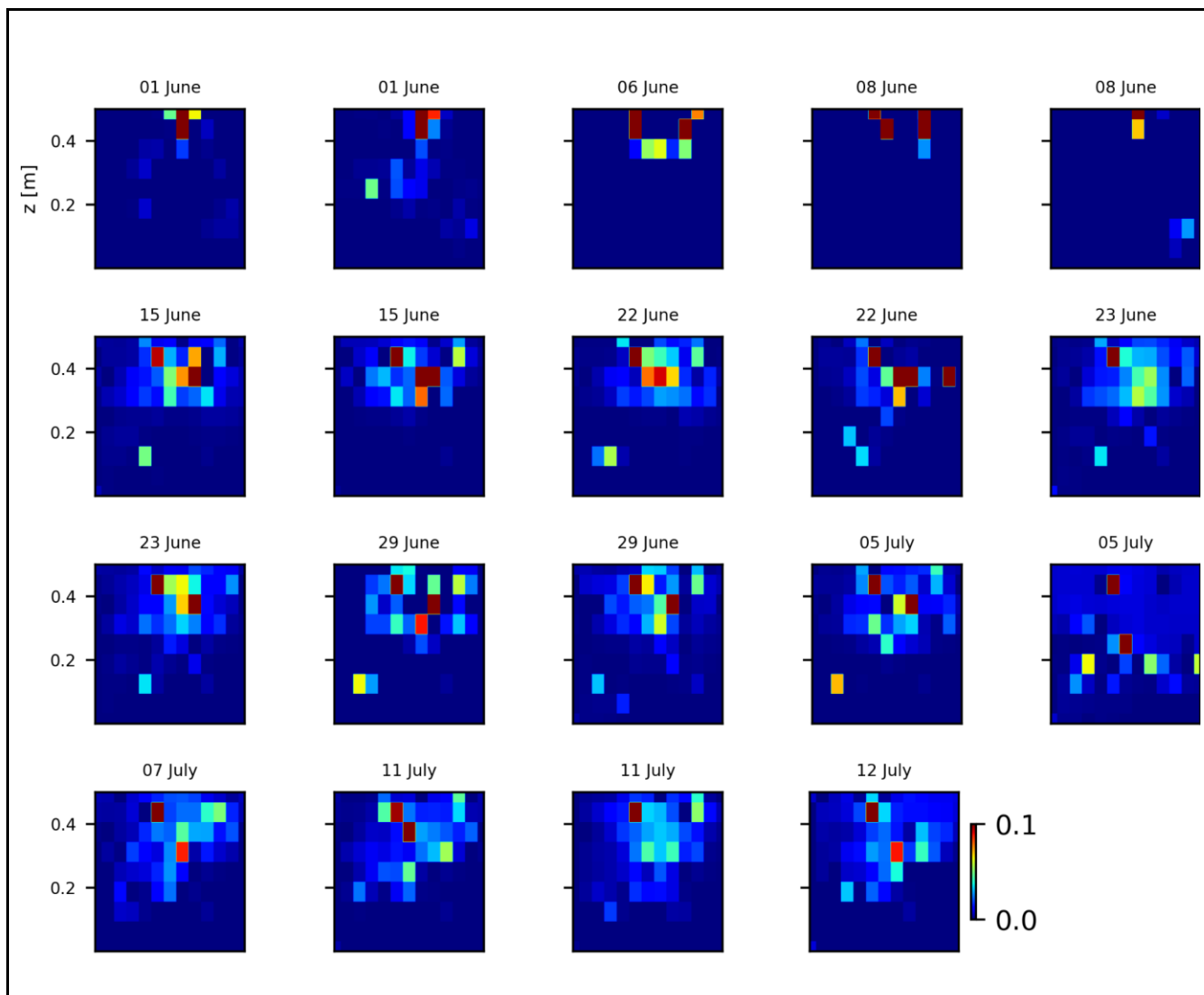
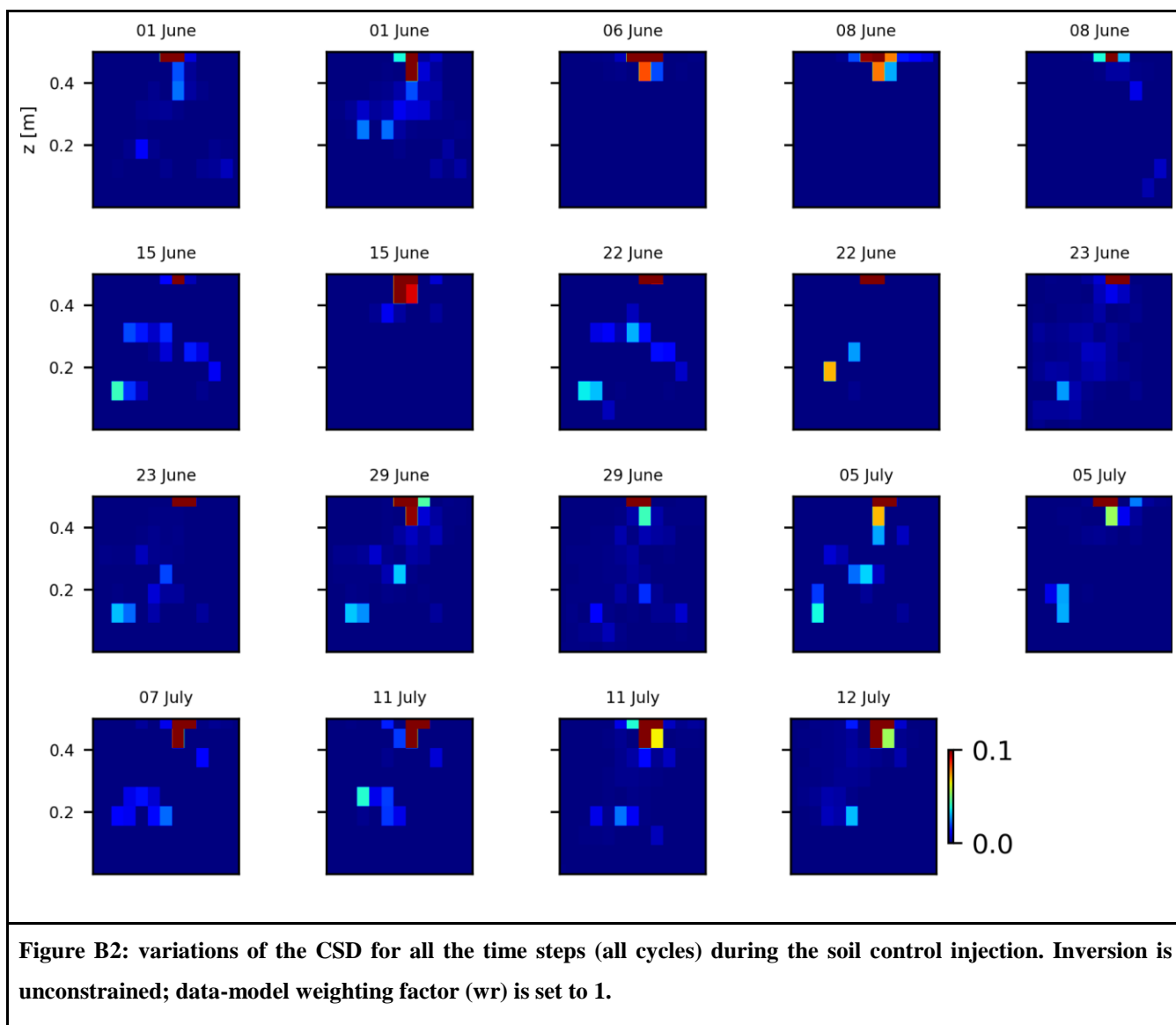


Figure B1: variations of the CSD for all the time steps (all cycles) during the stem injection. Inversion is unconstrained; data-model weighting factor (w_r) is set to 1.

743

744



745

746

747

748

749

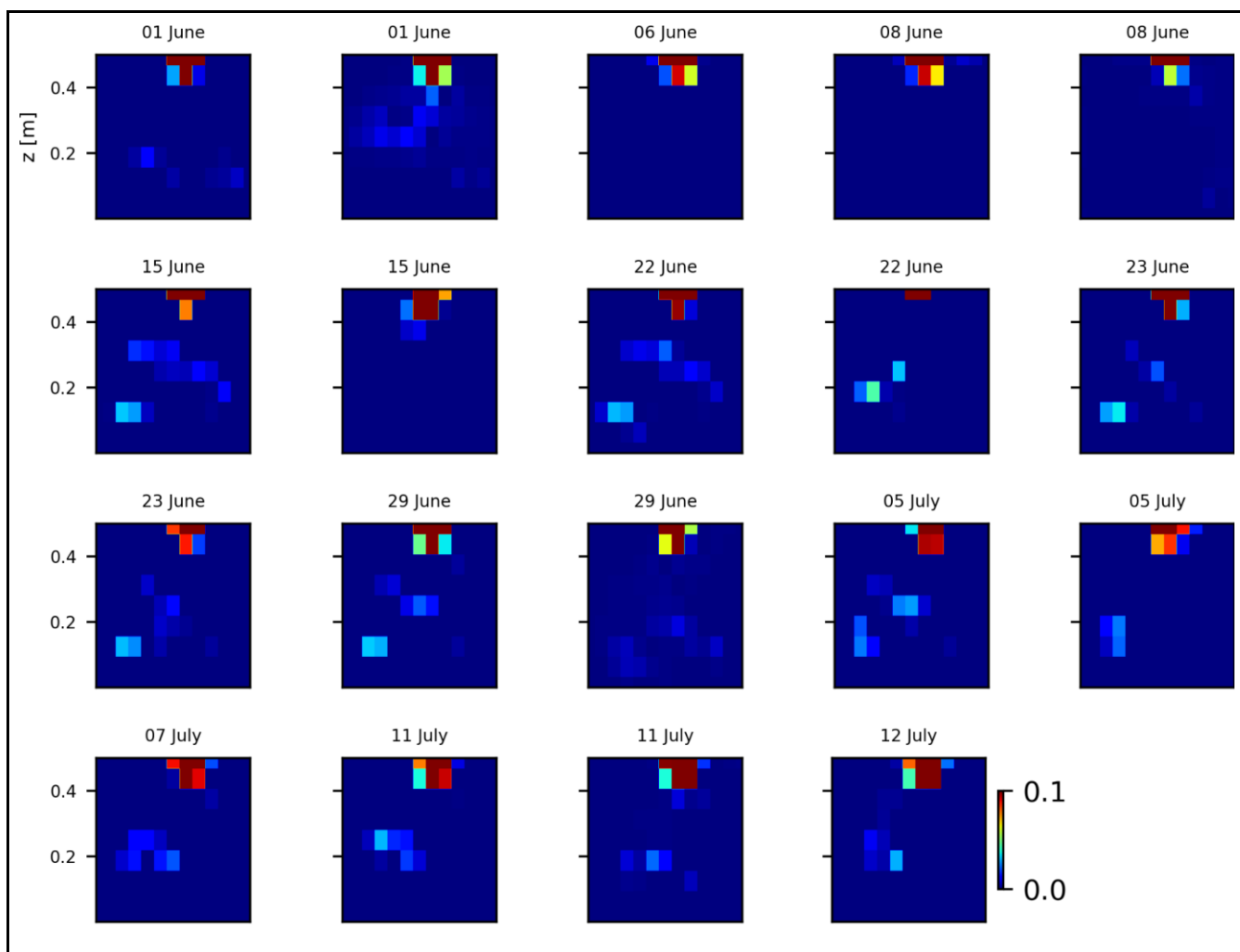


Figure B3: variations of the CSD for all the time steps (all cycles) during the soil control injection. Inversion is unconstrained; data-model weighting factor (w_r) is set to 10.

750

751

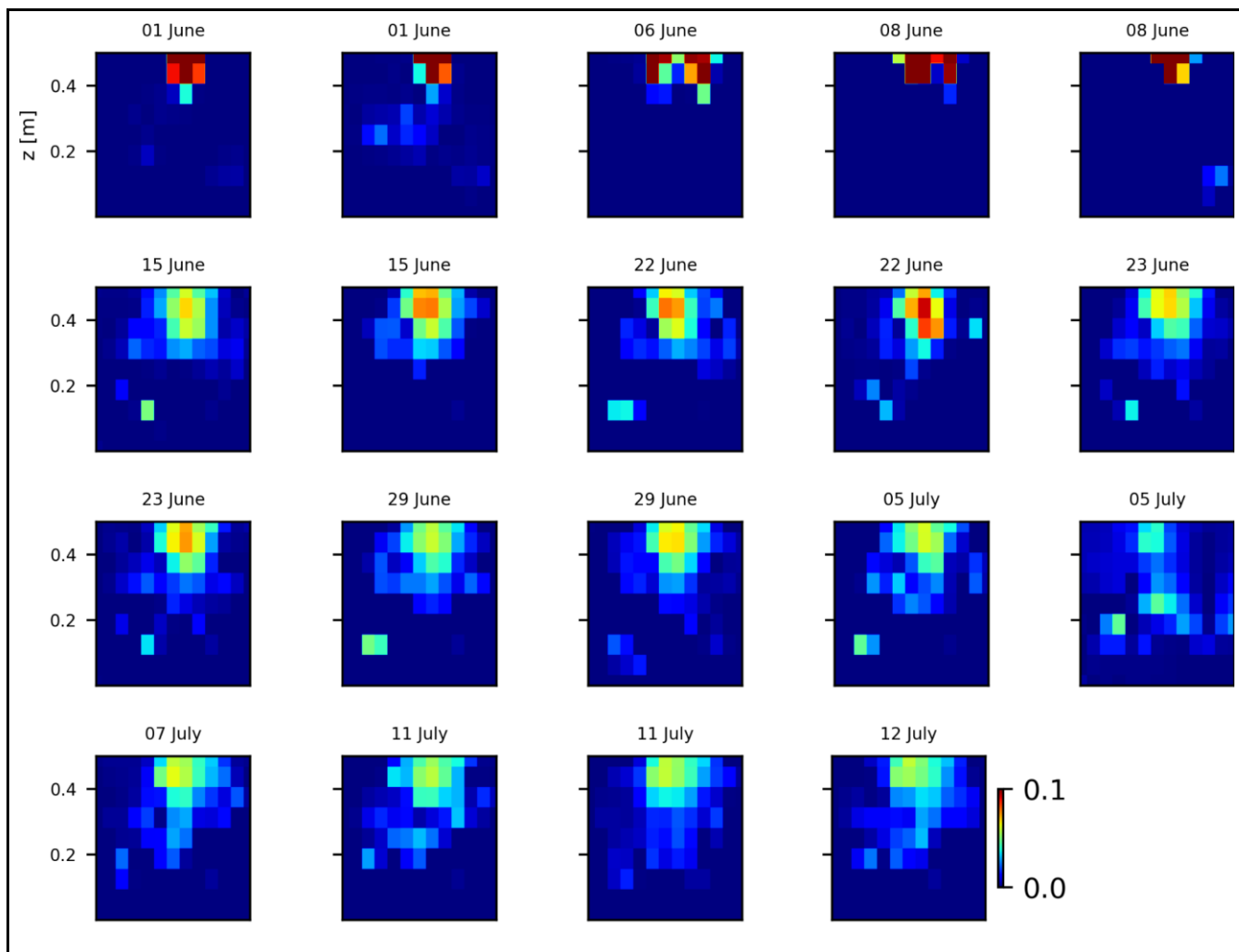


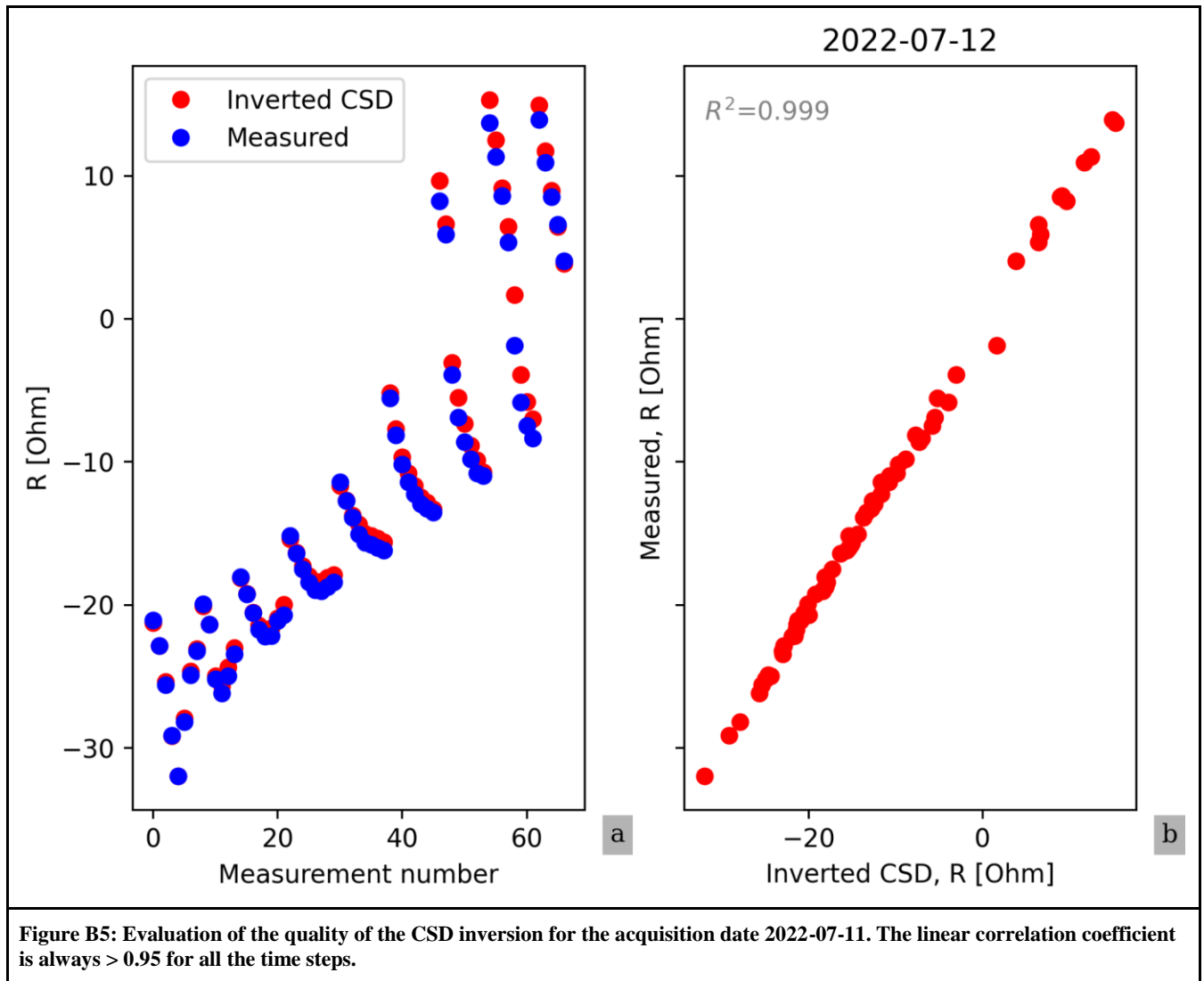
Figure B4: variations of the CSD for all the time steps (all cycles) during the stem injection. Inversion is unconstrained; data-model weighting factor (w_r) is set to 10.

752

753

754

755



756

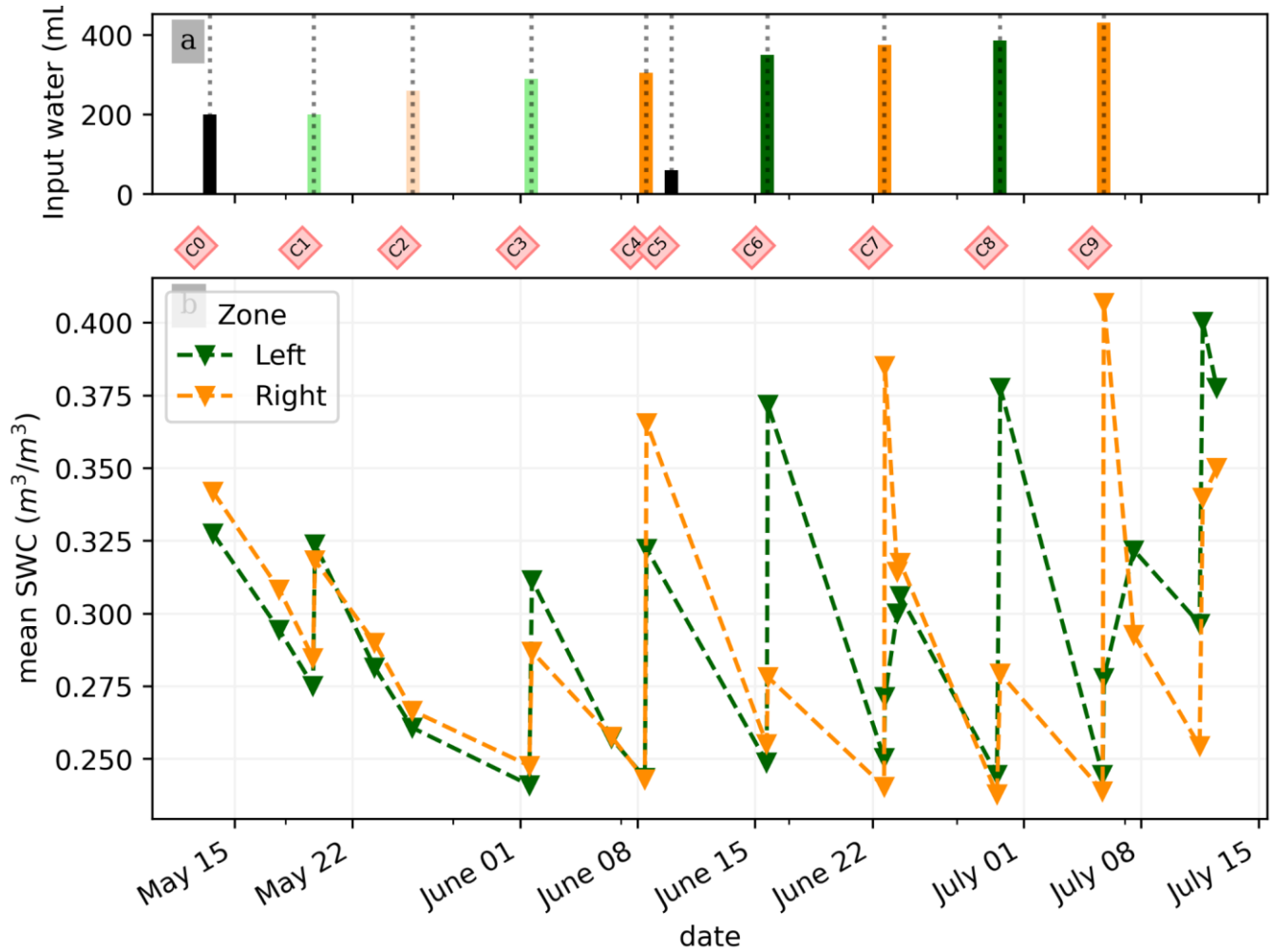
757

758

759 **Appendix C: Soil Water Content converted variations**

760

761



762

763 **Figure C1: (a) Evolution of the quantity (in mL) of water input spatially distributed with an alternate between left**
 764 **(green) and right (orange) during the PRD irrigation. The black bars hold for full-width irrigation (over all the holes,**
 765 **see fig. 1 manuscript), light green and orange bars hold for irrigation over the 4 sides of holes, and dark green/orange**

766 for 2 holes irrigation. (b) Evolution of the mean SWC (m³/m³) average on each side, markers show the acquisition
767 time.

768 7. Data availability

769 Codes and data to reproduce figures articles are available in the Zenodo data repository (link to come after decision).
770

771

772 *Competing interests*

773 The authors declare that they have no conflict of interest.
774

775 *Author contribution*

776 BM, VI, LP, FM, BR, CC, YW and GB designed the experiments, and BM, VI, BR and FM carried them out. BM, LP, GB ,
777 CC developed the model code and performed the simulations. BM prepared the manuscript with contributions from all co-
778 authors for writing – review & editing.
779

780

781 *Acknowledgments*

782 Benjamin Mary acknowledges the financial support from European Union’s Horizon 2020 research and innovation programme
783 under a Marie Skłodowska-Curie grant agreement (grant no. 842922).
784

785 References

- 786 1. Anonymous Reviewer: Comment on bg-2023-58, <https://doi.org/10.5194/bg-2023-58-RC2>, n.d.
- 787 2. Archie, G. E.: The Electrical Resistivity Log as an Aid in Determining Some Reservoir Characteristics, Trans. AIME,
788 146, 54–62, <https://doi.org/10.2118/942054-G>, 1942.
- 789 3. Binley, A.: 11.08 - Tools and Techniques: Electrical Methods, in: Treatise on Geophysics (Second Edition), edited
790 by: Schubert, G., Elsevier, Oxford, 233–259, <https://doi.org/10.1016/B978-0-444-53802-4.00192-5>, 2015.
- 791 4. Binley, A. and Slater, L.: Resistivity and induced polarization: theory and applications to the near-surface earth,
792 Cambridge University Press, Cambridge, UK ; New York, NY, 2020.

- 793 5. Blanchy, G., Saneiyani, S., Boyd, J., McLachlan, P., and Binley, A.: ResIPy, an intuitive open source software for
794 complex geoelectrical inversion/modeling, *Comput. Geosci.*, 137, 104423,
795 <https://doi.org/10.1016/j.cageo.2020.104423>, 2020.
- 796 6. Carminati, A. and Javaux, M.: Soil Rather Than Xylem Vulnerability Controls Stomatal Response to Drought, *Trends*
797 *Plant Sci.*, 25, 868–880, <https://doi.org/10.1016/j.tplants.2020.04.003>, 2020.
- 798 7. Cassiani, G., Boaga, J., Vanella, D., Perri, M. T., and Consoli, S.: Monitoring and modelling of soil–plant interactions:
799 the joint use of ERT, sap flow and eddy covariance data to characterize the volume of an orange tree root zone,
800 *Hydrol. Earth Syst. Sci.*, 19, 2213–2225, <https://doi.org/10.5194/hess-19-2213-2015>, 2015.
- 801 8. Cassiani, G., Boaga, J., Rossi, M., Putti, M., Fadda, G., Majone, B., and Bellin, A.: Soil–plant interaction monitoring:
802 Small scale example of an apple orchard in Trentino, North-Eastern Italy, *Science of The Total Environment*, 543,
803 851–861, <https://doi.org/10.1016/j.scitotenv.2015.03.113>, 2016.
- 804 9. Collins, M., Fuentes, S., and Barlow, E.: Partial rootzone drying and deficit irrigation increase stomatal sensitivity to
805 vapour pressure deficit in anisohydric grapevines, *Funct Plant Biol*, 37, 129–138, 2009.
- 806 10. Consoli, S., Stagno, F., Vanella, D., Boaga, J., Cassiani, G., and Rocuzzo, G.: Partial root-zone drying irrigation in
807 orange orchards: Effects on water use and crop production characteristics, *European Journal of Agronomy*, 82, 190–
808 202, <https://doi.org/10.1016/j.eja.2016.11.001>, 2017.
- 809 11. Cseresnyés, I., Vozáry, E., Kabos, S., and Rajkai, K.: Influence of substrate type and properties on root electrical
810 capacitance, *Int. Agrophysics*, 34, 95–101, <https://doi.org/10.31545/intagr/112147>, 2020.
- 811 12. Dalton, F. N.: In-situ root extent measurements by electrical capacitance methods, *Plant Soil*, 173, 157–165,
812 <https://doi.org/10.1007/BF00155527>, 1995.
- 813 13. Dietrich, S., Carrera, J., Weinzettel, P., and Sierra, L.: Estimation of Specific Yield and its Variability by Electrical
814 Resistivity Tomography, *Water Resour. Res.*, 54, 8653–8673, <https://doi.org/10.1029/2018WR022938>, 2018.
- 815 14. Doussan, C. and Garrigues, E.: Measuring and Imaging the Soil-root-water System with a Light Transmission 2D
816 Technique, *Bio-Protocol*, 9, <https://doi.org/10.21769/BioProtoc.3190>, 2019.

- 817 15. Düring, H., Dry, P. R., Botting, D. G., and Loveys, B.: Effects of partial root-zone drying on grapevine vigour, yield,
818 composition of fruit and use of water, in: Proceedings of the Ninth Australian Wine Industry Technical Conference :
819 Adelaide, South Australia, 16-19 July 1995, 1996, págs. 128-131, Proceedings of the Ninth Australian Wine Industry
820 Technical Conference : Adelaide, South Australia, 16-19 July 1995, 128–131, 1996.
- 821 16. Ehosioke, S., Nguyen, F., Rao, S., Kremer, T., Placencia-Gomez, E., Huisman, J. A., Kemna, A., Javaux, M., and
822 Garré, S.: Sensing the electrical properties of roots: A review, *Vadose Zone J.*, 19, e20082,
823 <https://doi.org/10.1002/vzj2.20082>, 2020.
- 824 17. Elsner, E. A. and Jubb, G. L.: Leaf Area Estimation of Concord Grape Leaves from Simple Linear Measurements,
825 *Am. J. Enol. Vitic.*, 39, 95–97, 1988.
- 826 18. Garré, S., Javaux, M., Vanderborght, J., Pagès, L., and Vereecken, H.: Three-dimensional electrical resistivity
827 tomography to monitor root zone water dynamics, *Vadose Zone Journal*, 10, 412–424,
828 <https://doi.org/10.2136/vzj2010.0079>, 2011.
- 829 19. Garré, S., Hyndman, D., Mary, B., and Werban, U.: Geophysics conquering new territories: The rise of
830 “agrogeophysics,” *Vadose Zone J.*, 20, e20115, <https://doi.org/10.1002/vzj2.20115>, 2021.
- 831 20. Garrigues, E., Doussan, C., and Pierret, A.: Water Uptake by Plant Roots: I – Formation and Propagation of a Water
832 Extraction Front in Mature Root Systems as Evidenced by 2D Light Transmission Imaging, *Plant Soil*, 283, 83–98,
833 <https://doi.org/10.1007/s11104-004-7903-0>, 2006.
- 834 21. Geuzaine, C. and Remacle, J.-F.: Gmsh: A 3-D finite element mesh generator with built-in pre- and post-processing
835 facilities, *Int. J. Numer. Methods Eng.*, 79, 1309–1331, <https://doi.org/10.1002/nme.2579>, 2009.
- 836 22. Gibert, D., Le Mouél, J.-L., Lambs, L., Nicollin, F., and Perrier, F.: Sap flow and daily electric potential variations in
837 a tree trunk, *Plant Science*, 171, 572–584, <https://doi.org/10.1016/j.plantsci.2006.06.012>, 2006.
- 838 23. Gimenez, C., Gallardo, M., and Thompson, R. B.: PLANT–WATER RELATIONS, in: *Encyclopedia of Soils in the*
839 *Environment*, edited by: Hillel, D., Elsevier, Oxford, 231–238, <https://doi.org/10.1016/B0-12-348530-4/00459-8>,
840 2005.

- 841 24. Gu, H., Liu, L., Butnor, J., Sun, H., Zhang, X., Li, C., and Liu, X.: Electrical capacitance estimates crop root traits
842 best under dry conditions—a case study in cotton (*Gossypium hirsutum* L.), *Plant Soil*, 467, 1–19,
843 <https://doi.org/10.1007/s11104-021-05094-6>, 2021.
- 844 25. Hoagland, D. R. and Arnon, D. I. (1950). The water culture method for growing plants without soil. *California Agric*
845 *Exp Stn Circ* 347: 1-32.
- 846 26. Jackisch, C., Knoblauch, S., Blume, T., Zehe, E., and Hassler, S. K.: Estimates of tree root water uptake from soil
847 moisture profile dynamics, *Biogeosciences*, 17, 5787–5808, <https://doi.org/10.5194/bg-17-5787-2020>, 2020.
- 848 27. Kamarajan, C., Pandey, A. K., Chorlian, D. B., and Porjesz, B.: The use of current source density as
849 electrophysiological correlates in neuropsychiatric disorders: a review of human studies, *Int. J. Psychophysiol. Off.*
850 *J. Int. Organ. Psychophysiol.*, 97, 310–322, <https://doi.org/10.1016/j.ijpsycho.2014.10.013>, 2015.
- 851 28. Liu, Y., Li, D., Qian, J., Di, B., Zhang, G., and Ren, Z.: Electrical impedance spectroscopy (EIS) in plant roots
852 research: a review, *Plant Methods*, 17, <https://doi.org/10.1186/s13007-021-00817-3>, 2021.
- 853 29. Lovisolo, C., Lavoie-Lamoureux, A., Tramontini, S., and Ferrandino, A.: Grapevine adaptations to water stress: new
854 perspectives about soil/plant interactions, *Theor. Exp. Plant Physiol.*, 28, 53–66, [https://doi.org/10.1007/s40626-016-](https://doi.org/10.1007/s40626-016-0057-7)
855 [0057-7](https://doi.org/10.1007/s40626-016-0057-7), 2016.
- 856 30. Malavasi, U. C., Davis, A. S., and Malavasi, M. de M.: Lignin in Woody Plants under Water Stress: A Review,
857 *Floresta E Ambiente*, 23, 589–597, <https://doi.org/10.1590/2179-8087.143715>, 2016.
- 858 31. Michot, D., Benderitter, Y., Dorigny, A., Nicoullaud, B., King, D., and Tabbagh, A.: Spatial and temporal monitoring
859 of soil water content with an irrigated corn crop cover using surface electrical resistivity tomography: Soil Water
860 Study Using Electrical Resistivity, *Water Resour. Res.*, 39, <https://doi.org/10.1029/2002WR001581>, 2003.
- 861 32. Mancuso, S. (Ed.): *Measuring roots: an updated approach*, Springer, Heidelberg ; New York, 382 pp., 2012.
- 862 33. Martin-Vertedor, A. I. and Dodd, I. C.: Root-to-shoot signalling when soil moisture is heterogeneous: increasing the
863 proportion of root biomass in drying soil inhibits leaf growth and increases leaf abscisic acid concentration: Root
864 distribution and non-hydraulic signalling, *Plant Cell Environ.*, 34, 1164–1175, [https://doi.org/10.1111/j.1365-](https://doi.org/10.1111/j.1365-3040.2011.02315.x)
865 [3040.2011.02315.x](https://doi.org/10.1111/j.1365-3040.2011.02315.x), 2011.

- 866 34. Mary, B., Peruzzo, L., Boaga, J., Schmutz, M., Wu, Y., Hubbard, S. S., and Cassiani, G.: Small-scale characterization
867 of vine plant root water uptake via 3-D electrical resistivity tomography and mise-à-la-masse method, *Hydrol. Earth*
868 *Syst. Sci.*, 22, 5427–5444, <https://doi.org/10.5194/hess-22-5427-2018>, 2018.
- 869 35. Mary, B., Vanella, D., Consoli, S., and Cassiani, G.: Assessing the extent of citrus trees root apparatus under deficit
870 irrigation via multi-method geo-electrical imaging, *Sci. Rep.*, 9, 9913, <https://doi.org/10.1038/s41598-019-46107-w>,
871 2019a.
- 872 36. Mary, B., Rao, S., Javaux, M., and Cassiani, G.: Tree root system mise-à-la-masse (MALM) forward modelling with
873 explicit representation of root structure., in: *Geophysical Research Abstracts*, 2019b.
- 874 37. McAdam, S. A. M., Sussmilch, F. C., and Brodribb, T. J.: Stomatal responses to vapour pressure deficit are regulated
875 by high speed gene expression in angiosperms, *Plant Cell Environ.*, 39, 485–491, <https://doi.org/10.1111/pce.12633>,
876 2016.
- 877 38. Parsekian, A. D., Claes, N., Singha, K., Minsley, B. J., Carr, B., Voytek, E., Harmon, R., Kass, A., Carey, A., Thayer,
878 D., and Flinchum, B.: Comparing Measurement Response and Inverted Results of Electrical Resistivity Tomography
879 Instruments, *J. Environ. Eng. Geophys.*, 22, 249–266, <https://doi.org/10.2113/JEEG22.3.249>, 2017.
- 880 39. Peruzzo, L., Chou, C., Wu, Y., Schmutz, M., Mary, B., Wagner, F. M., Petrov, P., Newman, G., Blancaflor, E. B.,
881 Liu, X., Ma, X., and Hubbard, S.: Imaging of plant current pathways for non-invasive root Phenotyping using a newly
882 developed electrical current source density approach, *Plant Soil*, 450, 567–584, [https://doi.org/10.1007/s11104-020-](https://doi.org/10.1007/s11104-020-04529-w)
883 [04529-w](https://doi.org/10.1007/s11104-020-04529-w), 2020.
- 884 40. Peruzzo, L., Liu, X., Chou, C., Blancaflor, E. B., Zhao, H., Ma, X.-F., Mary, B., Iván, V., Weigand, M., and Wu, Y.:
885 Three-channel electrical impedance spectroscopy for field-scale root phenotyping, *Plant Phenome J.*, 4, e20021,
886 <https://doi.org/10.1002/ppj2.20021>, 2021.
- 887 41. Postic, F. and Doussan, C.: Benchmarking electrical methods for rapid estimation of root biomass, *Plant Methods*,
888 12, 33, <https://doi.org/10.1186/s13007-016-0133-7>, 2016.

- 889 42. Rao, S., Meunier, F., Ehosioko, S., Lesparre, N., Kemna, A., Nguyen, F., Garré, S., and Javaux, M.: A mechanistic
890 model for electrical conduction in soil–root continuum: a virtual rhizotron study, *Biogeochemistry: Land*,
891 <https://doi.org/10.5194/bg-2018-280>, 2018.
- 892 43. Sartoni, R., Zegada-Lizarazu, W., and Monti, A.: A new compartmentalised rhizotron system for root phenotyping,
893 *Ital. J. Agron.*, 10, 53, <https://doi.org/10.4081/ija.2015.645>, 2015.
- 894 44. Sharp, R. E. and Davies, W. J.: Regulation of growth and development of plants growing with a restricted supply of
895 water, *Semin. Ser. - Soc. Exp. Biol.*, 1989.
- 896 45. Smart, D. R., Carlisle, E., Goebel, M., and Nunez, B. A.: Transverse hydraulic redistribution by a grapevine, *Plant*
897 *Cell Environ.*, 28, 157–166, <https://doi.org/10.1111/j.1365-3040.2004.01254.x>, 2005.
- 898 46. Song, C., Shen, W., Du, L., Wen, J., Lin, J., and Li, R.: Development and chemical characterization of Casparian
899 strips in the roots of Chinese fir (*Cunninghamia lanceolata*), *Trees*, 33, 827–836, [https://doi.org/10.1007/s00468-019-](https://doi.org/10.1007/s00468-019-01820-x)
900 01820-x, 2019.
- 901 47. Stoll, M.: Effects of partial rootzone drying on grapevine physiology and fruit quality, 2000.
- 902 48. Stoll, M., Loveys, B., and Dry, P.: Hormonal changes induced by partial rootzone drying of irrigated grapevine,
903 *Journal of Experimental Botany*, 51, 1627–1634, <https://doi.org/10.1093/jexbot/51.350.1627>, 2000.
- 904 49. Taylor, H. M., Upchurch, D. R., and McMichael, B. L.: Applications and limitations of rhizotrons and minirhizotrons
905 for root studies, *Plant Soil*, 129, 29–35, <https://doi.org/10.1007/BF00011688>, 1990.
- 906 50. Tsialtas, J. T., Koundouras, S., and Zioziou, E.: Leaf area estimation by simple measurements and evaluation of leaf
907 area prediction models in Cabernet-Sauvignon grapevine leaves, *Photosynthetica*, 46, 452–456,
908 <https://doi.org/10.1007/s11099-008-0077-x>, 2008.
- 909 51. Tsukanov, K. and Schwartz, N.: Relationship between wheat root properties and its electrical signature using the
910 spectral induced polarization method, *Vadose zone j.*, 19, <https://doi.org/10.1002/vzj2.20014>, 2020.
- 911 52. Tsukanov, K. and Schwartz, N.: Modeling Plant Roots Spectral Induced Polarization Signature, *Geophys. Res. Lett.*,
912 48, e2020GL090184, <https://doi.org/10.1029/2020GL090184>, 2021.

- 913 53. Uhlemann, S., Wilkinson, P. B., Maurer, H., Wagner, F. M., Johnson, T. C., and Chambers, J. E.: Optimized survey
914 design for electrical resistivity tomography: combined optimization of measurement configuration and electrode
915 placement, *Geophys. J. Int.*, 214, 108–121, <https://doi.org/10.1093/gji/ggy128>, 2018.
- 916 54. Urban, J., Bequet, R., and Mainiero, R.: Assessing the applicability of the earth impedance method for in situ studies
917 of tree root systems, *J. Exp. Bot.*, 62, 1857–1869, <https://doi.org/10.1093/jxb/erq370>, 2011.
- 918 55. Vanella D., G. Cassiani, L. Busato, J. Boaga, S. Barbagallo, A. Binley, S. Consoli, 2018, Use of small scale electrical
919 resistivity tomography to identify soil-root interactions during deficit irrigation, *Journal of Hydrology*, 556, 310-324,
920 doi: 10.1016/j.jhydrol.2017.11.025.
- 921 56. Virtanen, P., Gommers, R., Oliphant, T. E., Haberland, M., Reddy, T., Cournapeau, D., Burovski, E., Peterson, P.,
922 Weckesser, W., Bright, J., van der Walt, S. J., Brett, M., Wilson, J., Millman, K. J., Mayorov, N., Nelson, A. R. J.,
923 Jones, E., Kern, R., Larson, E., Carey, C. J., Polat, İ., Feng, Y., Moore, E. W., VanderPlas, J., Laxalde, D., Perktold,
924 J., Cimrman, R., Henriksen, I., Quintero, E. A., Harris, C. R., Archibald, A. M., Ribeiro, A. H., Pedregosa, F., and
925 van Mulbregt, P.: SciPy 1.0: fundamental algorithms for scientific computing in Python, *Nat. Methods*, 17, 261–272,
926 <https://doi.org/10.1038/s41592-019-0686-2>, 2020.
- 927 57. Voytek, E. B., Barnard, H. R., Jougnot, D., and Singha, K.: Transpiration- and precipitation-induced subsurface water
928 flow observed using the self-potential method, *Hydrol. Process.*, <https://doi.org/10.1002/hyp.13453>, 2019.
- 929 58. Whalley, W. R., Binley, A., Watts, C. W., Shanahan, P., Dodd, I. C., Ober, E. S., Ashton, R. W., Webster, C. P.,
930 White, R. P., and Hawkesford, M. J.: Methods to estimate changes in soil water for phenotyping root activity in the
931 field, *Plant Soil*, 415, 407–422, <https://doi.org/10.1007/s11104-016-3161-1>, 2017.
- 932 59. Weigand, M.: Monitoring Structural And Physiological Properties Of Crop Roots Using Spectral Electrical
933 Impedance Tomography, University of Bonn, 2017.
- 934 60. Weigand, M. and Kemna, A.: Imaging and functional characterization of crop root systems using spectroscopic
935 electrical impedance measurements, *Plant Soil*, 435, 201–224, <https://doi.org/10.1007/s11104-018-3867-3>, 2019.
- 936 61. Yan, J., Bogie, N. A., and Ghezzehei, T. A.: Root uptake under mismatched distributions of water and nutrients in
937 the root zone, *Biogeosciences*, 17, 6377–6392, <https://doi.org/10.5194/bg-17-6377-2020>, 2020.